

1 **Nitrate deposition and preservation in the snowpack along a traverse**  
2 **from coast to the ice sheet summit (Dome A) in East Antarctica**

3  
4 Guitao Shi<sup>1,2</sup>, Meredith G. Hastings<sup>3</sup>, Jinhai Yu<sup>2,4</sup>, Tianming Ma<sup>2,5</sup>, Zhengyi Hu<sup>2</sup>,  
5 Chunlei An<sup>2</sup>, Chuanjin Li<sup>6</sup>, Hongmei Ma<sup>2</sup>, Su Jiang<sup>2</sup>, and Yuansheng Li<sup>2</sup>

6  
7 <sup>1</sup> Key Laboratory of Geographic Information Science (Ministry of Education) and School of  
8 Geographic Sciences, East China Normal University, Shanghai 200241, China

9 <sup>2</sup> Key Laboratory for Polar Science of State Oceanic Administration, Polar Research Institute of China,  
10 Shanghai 200062, China

11 <sup>3</sup> Department of Earth, Environmental and Planetary Sciences and Institute at Brown for Environment  
12 and Society, Brown University, Providence, Rhode Island 02912, USA.

13 <sup>4</sup> School of Geographic and Oceanographic Sciences, Nanjing University, Nanjing 210023, China

14 <sup>5</sup> School of Ocean and Earth Science, Tongji University, Shanghai 200092, China

15 <sup>6</sup> The State Key Laboratory of the Cryospheric Sciences, Northwest Institute of Eco-Environment and  
16 Resources, Chinese Academy of Sciences, Lanzhou 730000, China

17  
18 *Correspondence to:* G. Shi (gt\_shi@163.com) and M.G. Hastings (meredith\_hastings@brown.edu)

19  
20  
21

22 **Abstract.** Antarctic ice core nitrate ( $\text{NO}_3^-$ ) can provide a unique record of the atmospheric reactive  
23 nitrogen cycle. However, the factors influencing the deposition and preservation of  $\text{NO}_3^-$  at the ice sheet  
24 surface must first be understood. Therefore, an intensive program of snow and atmospheric sampling  
25 was made on a traverse from the coast to the ice sheet summit, Dome A, East Antarctica. Snow samples  
26 in this observation include 120 surface snow samples (top ~3 cm), 20 snowpits with depths of 150 to  
27 300 cm, and 6 crystal ice samples (the topmost needle like layer on Dome A plateau). The main  
28 purpose of this investigation is to characterize the distribution pattern and preservation of  $\text{NO}_3^-$   
29 concentrations in the snow in different environments. Results show that an increasing trend of  $\text{NO}_3^-$   
30 concentrations with distance inland is present in surface snow, and  $\text{NO}_3^-$  is extremely enriched in the  
31 crystal ice (with a maximum of  $16.1 \mu\text{eq L}^{-1}$ ).  $\text{NO}_3^-$  concentration profiles for snowpits vary between  
32 coastal and inland sites. On the coast, the deposited  $\text{NO}_3^-$  was largely preserved, and the archived  $\text{NO}_3^-$   
33 fluxes are dominated by snow accumulation. The relationship between the archived  $\text{NO}_3^-$  and snow  
34 accumulation rate can be well depicted by a linear model, suggesting a homogeneity of atmospheric  
35  $\text{NO}_3^-$  levels. It is estimated that dry deposition contributes 27-44 % of the archived  $\text{NO}_3^-$  fluxes, and the  
36 dry deposition velocity and scavenging ratio for  $\text{NO}_3^-$  was relatively constant near the coast. Compared  
37 to the coast, the inland snow shows a relatively weak correlation between archived  $\text{NO}_3^-$  and snow  
38 accumulation, and the archived  $\text{NO}_3^-$  fluxes were more concentration dependent. The relationship  
39 between  $\text{NO}_3^-$  and coexisting ions ( $\text{nssSO}_4^{2-}$ ,  $\text{Na}^+$  and  $\text{Cl}^-$ ) was also investigated, and the results show a  
40 correlation between  $\text{nssSO}_4^{2-}$  (fine aerosol particles) and  $\text{NO}_3^-$  in surface snow, while the correlation  
41 between  $\text{NO}_3^-$  and  $\text{Na}^+$  (mainly associated with coarse aerosol particles) is not significant. In inland  
42 snow, there were no significant relationships found between  $\text{NO}_3^-$  and the coexisting ions, suggesting a  
43 dominant role of  $\text{NO}_3^-$  recycling in determining the concentrations.

44  
45  
46

## 1 Introduction

As the major sink of atmospheric nitrogen oxides ( $\text{NO}_x = \text{NO}$  and  $\text{NO}_2$ ), nitrate ( $\text{NO}_3^-$ ) is one of the major chemical species measured in polar snow and ice. The measurements of  $\text{NO}_3^-$  in ice cores may offer potential for understanding the complex atmospheric nitrogen cycle as well as oxidative capacity of the atmosphere through time (Legrand and Mayewski, 1997; Alexander et al., 2004; Hastings et al., 2009; Geng et al., 2017). However, the sources, transport pathways, and preservation of  $\text{NO}_3^-$  in Antarctic snowpack are still not well understood, hampering the interpretation of ice core  $\text{NO}_3^-$  records.

The accumulation of  $\text{NO}_3^-$  in snow is associated with various environmental factors and continental, tropospheric and stratospheric sources could influence  $\text{NO}_3^-$  concentrations (Legrand and Kirchner, 1990; McCabe et al., 2007; Wolff et al., 2008; Lee et al., 2014). In surface snow,  $\text{NO}_3^-$  levels are thought to be linked with snow accumulation rate, and higher values are usually present in areas with low accumulation, e.g., East Antarctic plateaus (Qin et al., 1992; Erbland et al., 2013; Traversi et al., 2017). Unlike sea salt related ions (e.g., chloride ( $\text{Cl}^-$ ), sodium ( $\text{Na}^+$ ), and occasionally sulfate ( $\text{SO}_4^{2-}$ )),  $\text{NO}_3^-$  does not usually show an elevated level in coastal Antarctic snow (Mulvaney and Wolff, 1994; Bertler et al., 2005; Frey et al., 2009), suggesting a negligible contribution from sea salt aerosols. However, the marine emissions of alkyl  $\text{NO}_3^-$ , particularly methyl and ethyl  $\text{NO}_3^-$ , produced in surface oceans by microbiological and/or photochemical processes, are thought to be a possible contribution to Antarctic  $\text{NO}_3^-$  (Jones et al., 1999; Liss et al., 2004). At Halley station in coastal Antarctica, significant concentrations of organic nitrates (peroxyacetyl nitrate (PAN) and alkyl  $\text{NO}_3^-$ ) were observed in the lower atmosphere (Jones et al., 2011). Organic nitrates dominated the  $\text{NO}_y$  (sum of reactive nitrogen oxide compounds) budget during the winter, and were on par with inorganic nitrate compounds during the summer. Although not a direct source of snowpack nitrate, organic nitrates could act as source of  $\text{NO}_x$  to coastal Antarctica that would ultimately contribute to  $\text{NO}_3^-$  within the snowpack (Jones et al., 2011).

While industrial and/or agricultural emissions have contributed to increasing  $\text{NO}_3^-$  levels in Greenland snow and ice over recent decades to hundreds of years, the anthropogenic contribution to Antarctic  $\text{NO}_3^-$  is less clear (Mayewski and Legrand, 1990; Hastings et al., 2009; Felix and Elliott, 2013; Geng et al., 2014). Lightning and  $\text{NO}_x$  produced in the lower stratosphere have long been thought to play a major role (Legrand et al., 1989; Legrand and Kirchner, 1990). Recently, adjoint model simulations proposed that tropospheric transport of  $\text{NO}_3^-$  from mid-low latitude  $\text{NO}_x$  sources is an important source to the Antarctic year round, though less so in austral spring/summer (Lee et al., 2014). A recent treatment of  $\text{NO}_3^-$  in snow in the same global chemical transport model suggests that the recycling of  $\text{NO}_3^-$  and/or transport of  $\text{NO}_x$  due to photolysis of  $\text{NO}_3^-$  in the surface snow layer is important in determining summertime concentrations (Zatko et al., 2016). The stratospheric inputs of  $\text{NO}_3^-$  are thought to result from  $\text{N}_2\text{O}$  oxidation to  $\text{NO}$ , then formation of  $\text{NO}_3^-$  that is deposited via polar stratospheric cloud (PSC) sedimentation (Legrand et al., 1989; Legrand and Kirchner, 1990). The late winter/early spring secondary maximum of  $\text{NO}_3^-$  observed in the atmosphere at coastal and inland locations has been attributed to the stratospheric source based on the  $\text{NO}_3^-$  stable isotopic composition (Legrand et al., 1989; Savarino et al., 2007; Frey et al., 2009). At some sites, the snow/ice core  $\text{NO}_3^-$  concentrations were found to be linked with regional atmospheric circulation (e.g., sea level pressure gradient; Goodwin et al., 2003; Russell et al., 2006). In general, atmospheric circulation appears not to affect snow  $\text{NO}_3^-$  concentrations directly, but indirectly through an influence on the air mass transport and/or snow accumulation rate (Russell et al., 2004; Russell et al., 2006). In addition, while some

91 studies suggested that snow/ice  $\text{NO}_3^-$  is possibly linked with extraterrestrial fluxes of energetic particles  
92 and solar irradiation, with solar flares corresponding to  $\text{NO}_3^-$  spikes (Zeller et al., 1986; Smart et al.,  
93 2014), other observations and recent modeling studies have established that there is not a clear  
94 connection between solar variability and  $\text{NO}_3^-$  concentrations (Legrand et al., 1989; Legrand and  
95 Kirchner, 1990; Wolff et al., 2008; Wolff et al., 2012; Duderstadt et al., 2014; Duderstadt et al., 2016;  
96 Wolff et al., 2016). However, the potential link between the long-term (e.g., centennial to millennial  
97 time scales) variability of  $\text{NO}_3^-$  and solar cycles may be present at some locations (Traversi et al., 2012).  
98 In summary, factors influencing  $\text{NO}_3^-$  levels in snow/ice are complicated, and the significance of the  
99 relationship between  $\text{NO}_3^-$  and controlling factors varies temporally and spatially.

100 Gas phase and snow concentration studies, and recent isotopic investigations and modeling have  
101 shown that  $\text{NO}_3^-$ , particularly in snow on the Antarctic plateau, is a combination of deposition of  $\text{HNO}_3$   
102 and post-depositional loss or recycling of  $\text{NO}_3^-$  (e.g., Röhrlisberger et al., 2002; Davis et al., 2004;  
103 Dibb et al., 2004; Erbland et al., 2013; Erbland et al., 2015; Shi et al., 2015; Bock et al., 2016; Zatko et  
104 al., 2016). Based upon a suite of isotopic studies in the field and laboratory, it has been demonstrated  
105 that under cold, sunlit conditions ultraviolet photolysis dominates  $\text{NO}_3^-$  post-depositional processing,  
106 whereas  $\text{HNO}_3$  volatilization may become more important at warmer temperatures  $> -20$  °C  
107 (Röhrlisberger et al., 2002; Frey et al., 2009; Erbland et al., 2013; Berhanu et al., 2015). In snowpack,  
108 the solar radiation decreases exponentially, with attenuation described in terms of an  $e$ -folding depth ( $z_e$ )  
109 where the actinic flux is reduced to 37 % (i.e.,  $1/e$ ) of the surface value. Thus, about 95 % of snowpack  
110 photochemistry is expected to occur above the depth of three times  $z_e$  (Warren et al., 2006). Field  
111 measurements at Dome C on the East Antarctic plateau suggest a  $z_e$  of 10 to 20 cm (France et al., 2011),  
112 and the depth is dependent upon the concentration of impurities contained in the snow (Zatko et al.,  
113 2013). In the inland regions with low snow accumulation rates, particularly on the East Antarctic  
114 plateaus, photolysis has been shown to lead to significant post-depositional loss of  $\text{NO}_3^-$ , demonstrated  
115 by significant enrichment in  $^{15}\text{N}$  of snow  $\text{NO}_3^-$  (i.e., high  $\delta^{15}\text{N}$ ) (Frey et al., 2009; Erbland et al., 2013;  
116 Berhanu et al., 2015; Erbland et al., 2015; Shi et al., 2015), as well as a decrease in  $\delta^{18}\text{O}$  and  $\Delta^{17}\text{O}$  due  
117 to reformation of  $\text{NO}_3^-$  in the condensed phase (Erbland et al., 2013; Shi et al., 2015 and references  
118 therein). The transport and recycling of  $\text{NO}_x$  sourced from photolysis of snow  $\text{NO}_3^-$  in the summertime  
119 has been invoked to model the distribution of snowpack  $\text{NO}_3^-$  across the Antarctic plateau (Zatko et al.,  
120 2016). However, snow physical characteristics play a crucial role in  $\text{NO}_3^-$  deposition and preservation.  
121 For instance, summertime concentrations in the surface skin layer of snow (the uppermost ~4 mm) can  
122 be explained as the result of co-condensation of  $\text{HNO}_3$  and water vapour, with little to no photolytic  
123 loss in this microlayer (Bock et al., 2016). The combination of concentration and isotopic studies, along  
124 with physical aspects of the snow, could lead to the reconstruction and interpretation of atmospheric  
125  $\text{NO}_3^-$  over time (e.g., Erbland et al., 2015; Bock et al., 2016), if there is detailed understanding of the  
126  $\text{NO}_3^-$  deposition and preservation in different environments in Antarctica.

127 The effects of volatilization of  $\text{NO}_3^-$  are uncertain, given that one field experiment suggests that this  
128 process is an active player in  $\text{NO}_3^-$  loss (17 % (-30 °C) to 67 % (-10 °C) of  $\text{NO}_3^-$  lost after two weeks'  
129 physical release experiments; Erbland et al., 2013), while other laboratory and field studies show that  
130 volatilization plays a negligible role in  $\text{NO}_3^-$  loss (Berhanu et al., 2014; Berhanu et al., 2015). Further  
131 investigations are needed to quantify the effects of volatilization for a better understanding of  $\text{NO}_3^-$   
132 preservation in snow/ice. Based on  $z_e$ ,  $\text{NO}_3^-$  at deeper depths in Antarctic snow (e.g.,  $> 100$  cm), well  
133 beyond the snow photic zone, may be taken as the archived fraction. Thus,  $\text{NO}_3^-$  in deeper snow  
134 possibly provides an opportunity to investigate the archived fraction and potential influencing factors

135 (e.g., snow accumulation rate). Given that an extensive array of ice core measurements is unavailable  
136 in most of Antarctica, the deeper snowpits (with depth > 100 cm) may offer a useful way to investigate  
137 the archived  $\text{NO}_3^-$ .

138 In the atmosphere in Antarctica, particularly during spring and summer,  $\text{NO}_3^-$  is found to be mainly  
139 in the form of gas phase  $\text{HNO}_3$ , with  $\text{NO}_3^-$  concentration several times higher in gas phase than in the  
140 particulate phase (Piel et al., 2006; Legrand et al., 2017b; Traversi et al., 2017). During  
141 post-depositional processes, the uptake of gaseous  $\text{HNO}_3$  is thought to be important in  $\text{NO}_3^-$   
142 concentrations in surface snow layers (Udisti et al., 2004; Traversi et al., 2014; Traversi et al., 2017).  
143 Due to the high concentration in summer,  $\text{HNO}_3$  appears to play an important role in acidifying sea-salt  
144 particles, possibly accounting for the presence of  $\text{NO}_3^-$  in the particulate phase in summer (Jourdain and  
145 Legrand, 2002; Legrand et al., 2017b; Traversi et al., 2017). It is noted that the significant increase of  
146  $\text{NO}_3^-$  during the cold periods (e.g., Last Glacial Maximum) could be associated with its attachment to  
147 dust aerosol, instead of formation of gas phase  $\text{HNO}_3$  (Legrand et al., 1999; Wolff et al., 2010).

148 To date, investigations on spatial and temporal patterns of snow  $\text{NO}_3^-$  have been performed on  
149 several traverses in Antarctica (e.g., 1990 International Trans-Antarctica Expedition, and DDU to  
150 Dome C; Qin et al., 1992; Bertler et al., 2005; Frey et al., 2009; Erbland et al., 2013; Pasteris et al.,  
151 2014), but these provide an uneven distribution of snow  $\text{NO}_3^-$  concentrations and leave large regions  
152 un-sampled (e.g., Lambert Glacier basin and Dome A plateau). Over the past few decades, while  
153 several glaciological observations have been carried out on the Chinese inland Antarctic traverse route  
154 from Zhongshan to Dome A, East Antarctica (Hou et al., 2007; Ding et al., 2010; Ma et al., 2010; Ding  
155 et al., 2011; Li et al., 2013; Shi et al., 2015), the data on snow chemistry are still rare, particularly  
156 detailed information on  $\text{NO}_3^-$ . From 2009 to 2013, we therefore conducted surface snow and snowpit  
157 sampling campaigns along the traverse route, with the main objectives to (1) describe  $\text{NO}_3^-$  distribution  
158 in surface snow and snowpits, (2) characterize the relationship between archived  $\text{NO}_3^-$  and snow  
159 accumulation rate, and (3) examine the potential effects of coexisting ions on  $\text{NO}_3^-$  preservation. The  
160 results of this study may help to better understand  $\text{NO}_3^-$  deposition and preservation in the snowpack,  
161 which is critical to the interpretation of ice core  $\text{NO}_3^-$  records.

162

## 163 **2 Methodology**

164

### 165 **2.1 Study area (Zhongshan to Dome A traverse)**

166 The Zhongshan to Dome A CHINARE (Chinese National Antarctic Research Expedition) inland  
167 traverse is an important leg of the ITASE (International Trans-Antarctic Scientific Expedition). The  
168 traverse is in the Indian Ocean sector of East Antarctica, passing through the Lambert Glacier, the  
169 largest glacier in Antarctica. In January 1997 the first Chinese Antarctic inland expedition reached an  
170 area ~300 km from the coast; in January 1998 the traverse was extended to 464 km, and in December  
171 1998, to the Dome A area ~1100 km from the coast. In the austral 2004/2005 summer for the first time,  
172 the traverse extended to the ice sheet summit, Dome A, a total distance of ~1260 km. In January 2009,  
173 the Chinese inland research base, Kunlun station (80°25'1.7"S and 77°6'58.0"E, 4087 m above mean  
174 sea level), was established at Dome A, mainly aimed at deep ice core drilling and astronomical  
175 observations. Now, Kunlun base is a summer station, and the CHINARE team typically conducts an  
176 annual inland traverse from the coastal Zhongshan station to Dome A.

177 In January 2010, the Dome A deep ice core project was started, and the construction of basic  
178 infrastructure (including drill trench and scientific workroom) took 4 summer seasons. The deep ice

179 core drilling began in January 2013, and in total 801 m ice core was recovered by the 2016/2017 season.  
180 The investigation of  $\text{NO}_3^-$  deposition and preservation in the snowpack will be of help to the  
181 interpretation of Dome A deep ice core  $\text{NO}_3^-$  records.

182

## 183 2.2 Sample collection

184 During the 2010/2011 CHINARE, surface snow samples (the topmost ~3 cm) were collected at an  
185 interval of ~10 km along the traverse route from Zhongshan to Dome A, using 3.0 cm diameter  
186 high-density polyethylene (HDPE) bottles (volume = 100 ml). The bottles were pre-cleaned with  
187 Milli-Q ultrapure water (18.2 M $\Omega$ ), until electrical conductivity of the water stored in bottles (> 24 h)  
188 decreased to <0.5  $\mu\text{S cm}^{-1}$ . Then, the bottles were dried under a class 100 super clean hood at 20 °C.  
189 Immediately after the drying procedure, the bottles were sealed in clean PE bags that were not opened  
190 until the field sampling started. At each sampling site (typically > 500 m away from the traverse route),  
191 the bottles were pushed into surface snow layers in the windward direction. In total, 120 surface snow  
192 samples were collected. In addition, at each sampling site, the upper snow density (~10 cm) was  
193 measured using a density scoop with a volume of 1000  $\text{cm}^3$ . As the field blanks, pre-cleaned bottles  
194 filled with Milli-Q water were taken to the field and treated to the same conditions as field samples ( $n =$   
195 3).

196 On the Dome A plateau, the snow is soft and non-cohesive, and morphology of the surface snow is  
197 different from other areas on the traverse, with a needle ice crystal layer extensively developed, in  
198 particular on the sastrugi (Fig. S1 in supporting information). The depth of the needle-like crystal ice  
199 layer (referred to as “crystal ice” in the following context) is generally < 1.0 cm. In order to investigate  
200 air-snow transfer of  $\text{NO}_3^-$  in this uppermost ~1 cm layer, the crystal ice was collected using a clean  
201 HDPE scoop, and then poured into clean wide mouth HDPE bottles. Approximately 30 g of crystal ice  
202 was collected for each sample. In total, 6 crystal ice samples were collected on the traverse near Dome  
203 A plateau.

204 In addition to surface snow, snowpit samples were collected during CHINARE inland traverse  
205 campaigns in 2009/2010, 2010/2011, and 2012/2013. The snowpits were excavated manually, and the  
206 snow wall in the windward direction was scraped clean and flat with a clean HDPE scraper. Then the  
207 bottles were pushed horizontally into the snow wall. Snowpit samples were collected from the base  
208 towards the top layer along a vertical line. During the sampling process, all personnel wore PE gloves  
209 and facemasks to minimize potential contamination. Note that the snowpits are generally > 1 km from  
210 the traverse route to avoid possible contamination from the expedition activities. The full information  
211 about individual snowpits, including location, distance from the coast, elevation, snowpit depth,  
212 sampling resolution, collection date, and annual snow accumulation rate, is summarized in Table 1. All  
213 together, 20 snowpits (SP1 to SP20 in Fig. 2, with SP20 corresponding to the location of Kunlun  
214 station at Dome A) as 1741 snow samples, were collected.

215 To support understanding of the air-snow transfer of  $\text{NO}_3^-$  on the traverse, atmospheric  $\text{NO}_3^-$  was  
216 collected on glass fiber filters (Whatman G653) using a high volume air sampler (HVAS), with a flow  
217 rate of ~1.0  $\text{m}^3 \text{min}^{-1}$  for 12-15 hr, during the inland traverse campaign in 2015/2016. The  $\text{NO}_3^-$   
218 collected on glass fiber filters are expected to equal the sum of particulate  $\text{NO}_3^-$  and gaseous  $\text{HNO}_3$ ,  
219 based upon previous investigations in East Antarctica (Savarino et al., 2007; Frey et al., 2009; Erbland  
220 et al., 2013). In total, 34 atmospheric samples were collected on the traverse. In addition, two field  
221 blanks were collected from filters installed in the HVAS without pumping and treated as samples  
222 thereafter. Detailed information about the atmospheric sampling is presented in Table S1 in supporting

223 information.

224 After sample collection, all filters and snow samples were sealed in clean PE bags and preserved in  
225 clean thermal insulated boxes. All of the samples were transported to the laboratory under freezing  
226 conditions ( $< -20\text{ }^{\circ}\text{C}$ ).

227

### 228 2.3 Sample analysis

229 In the laboratory, three quarters of individual filters were cut into pieces using pre-cleaned scissors  
230 that were rinsed between samples, placed in  $\sim 100$  ml of Milli-Q water, ultrasonicated for 40 min and  
231 leached for 24 hr under shaking. The sample solutions were then filtered through  $0.22\text{ }\mu\text{m}$  ANPEL  
232 PTFE filters for concentration analysis. Snow samples were melted in the closed sampling bottles on a  
233 super clean bench (class 100) before chemical measurements. Analyses of  $\text{Na}^+$ ,  $\text{NH}_4^+$ ,  $\text{K}^+$ ,  $\text{Mg}^{2+}$ ,  $\text{Ca}^{2+}$ ,  
234  $\text{Cl}^-$ ,  $\text{NO}_3^-$  and  $\text{SO}_4^{2-}$  were performed using a Dionex ICS-3000 ion chromatography system. The column  
235 used for cation analysis ( $\text{Na}^+$ ,  $\text{NH}_4^+$ ,  $\text{K}^+$ ,  $\text{Mg}^{2+}$  and  $\text{Ca}^{2+}$ ) was a Dionex column CS12 ( $2\times 250$  mm), with  
236 a guard column CG12 ( $2\times 50$  mm); while the anions ( $\text{Cl}^-$ ,  $\text{NO}_3^-$  and  $\text{SO}_4^{2-}$ ) were analyzed using a  
237 Dionex column AS11 ( $2\times 250$  mm) with a guard column AG11 ( $2\times 50$  mm). The eluent for cations was  
238  $18.0\text{ mM}$  methanesulfonic acid (MSA), and the gradient elution method was employed for anion  
239 analysis, with eluent of potassium hydroxide (KOH). More details on this method are described in a  
240 previous report (Shi et al., 2012). During sample analysis, duplicated samples and field blanks were

241 synchronously analyzed. The pooled standard deviation ( $\sigma_p$ ,  $\sigma_p = \sqrt{\sum_{i=1}^k (n_i - 1)s_i^2 / \sum_{i=1}^k (n_i - 1)}$ ,

242 where  $n_i$  and  $s_i^2$  are the size and variance of the  $i$ th samples respectively, and  $k$  is the total number of  
243 sample sets) of all replicate samples run at least twice in two different sample sets is  $0.019$  ( $\text{Cl}^-$ ),  $0.023$   
244 ( $\text{NO}_3^-$ ),  $0.037$  ( $\text{SO}_4^{2-}$ ),  $0.022$  ( $\text{Na}^+$ ),  $0.039$  ( $\text{NH}_4^+$ ),  $0.006$  ( $\text{K}^+$ ),  $0.006$  ( $\text{Mg}^{2+}$ ) and  $0.006$  ( $\text{Ca}^{2+}$ )  $\mu\text{eq L}^{-1}$   
245 respectively ( $n = 65$  pairs of samples). Ion concentrations in field blanks ( $n = 3$ ) are generally lower  
246 than the detection limit (DL, 3 standard deviations of water blank in the laboratory).

247 For Antarctic snow samples, the concentrations of  $\text{H}^+$  are usually not measured directly, but deduced  
248 from the ion-balance disequilibrium in the snow. Here,  $\text{H}^+$  concentration is calculated through ion  
249 balance.

$$250 [\text{H}^+] = [\text{Cl}^-] + [\text{NO}_3^-] + [\text{SO}_4^{2-}] - [\text{Na}^+] - [\text{NH}_4^+] - [\text{Mg}^{2+}] - [\text{Ca}^{2+}] \text{ (Eq. 1),}$$

251 where ion concentrations are in  $\mu\text{eq L}^{-1}$ . In addition, the non-sea salt fractions of  $\text{SO}_4^{2-}$  ( $\text{nssSO}_4^{2-}$ ) and  
252  $\text{Cl}^-$  ( $\text{nssCl}^-$ ) can be calculated from the following expressions, by assuming  $\text{Na}^+$  exclusively from sea  
253 salt (in  $\mu\text{eq L}^{-1}$ ).

$$254 [\text{nssSO}_4^{2-}] = [\text{SO}_4^{2-}] - 0.12 \times [\text{Na}^+] \text{ (Eq. 2),}$$

$$255 [\text{nssCl}^-] = [\text{Cl}^-] - 1.17 \times [\text{Na}^+] \text{ (Eq. 3).}$$

256 It is noted that  $\text{SO}_4^{2-}$  fractionation (the precipitation of mirabilite ( $\text{Na}_2\text{SO}_4 \cdot 10\text{H}_2\text{O}$ )) may introduce a  
257 bias in  $\text{nssSO}_4^{2-}$ , particularly during the winter half year (Wagenbach et al., 1998a).

258

## 259 3 Results

260

### 261 3.1 $\text{NO}_3^-$ concentration in surface snow

262 Concentrations of  $\text{NO}_3^-$  in surface snow are shown in Fig. 1, ranging from  $0.6$  to  $5.1\text{ }\mu\text{eq L}^{-1}$ , with a  
263 mean of  $2.4\text{ }\mu\text{eq L}^{-1}$ . One standard deviation ( $1\sigma$ ) of  $\text{NO}_3^-$  concentration in surface snow is  $1.1\text{ }\mu\text{eq L}^{-1}$ ,  
264 with coefficient of variation ( $C_v$ ,  $1\sigma$  over mean) of  $0.5$ , indicating a moderate spatial variability. On the  
265 coastal  $\sim 450$  km,  $\text{NO}_3^-$  shows a slightly increasing trend towards the interior, with low variability, while

266 NO<sub>3</sub><sup>-</sup> concentrations are higher in the inland region, with a large fluctuation. It is notable that in the  
267 area ~800 km from the coast, where snow accumulation is relatively high, NO<sub>3</sub><sup>-</sup> concentrations  
268 decrease to < 2.0 µeq L<sup>-1</sup>, comparable to the values on the coast. Near the Dome A plateau (> 1000 km  
269 from coast), there is a tendency for higher NO<sub>3</sub><sup>-</sup> concentrations (> 5.0 µeq L<sup>-1</sup>). Similarly, atmospheric  
270 NO<sub>3</sub><sup>-</sup> concentrations increase from the coast towards the plateau, ranging from 6 to 118 ng m<sup>-3</sup> (mean =  
271 38 ng m<sup>-3</sup>) (Fig. 1).

272 The percentage that surface snow NO<sub>3</sub><sup>-</sup> contributes to total ions (i.e., total ionic strength, sum of Na<sup>+</sup>,  
273 NH<sub>4</sub><sup>+</sup>, K<sup>+</sup>, Mg<sup>2+</sup>, Ca<sup>2+</sup>, Cl<sup>-</sup>, NO<sub>3</sub><sup>-</sup>, SO<sub>4</sub><sup>2-</sup> and H<sup>+</sup>, in µeq L<sup>-1</sup>) varies from 6.7 to 37.6 % (mean = 27.0 %;  
274 Fig. S2 in supporting information), with low values near the coast and high percentages on the plateau.  
275 A strong relationship was found between NO<sub>3</sub><sup>-</sup> and the total ionic strength in surface snow ( $R^2 = 0.55$ ,  $p$   
276 < 0.01).

277 In the crystal ice, the means (ranges) of Cl<sup>-</sup>, NO<sub>3</sub><sup>-</sup>, SO<sub>4</sub><sup>2-</sup>, Na<sup>+</sup>, NH<sub>4</sub><sup>+</sup>, K<sup>+</sup>, Mg<sup>2+</sup>, Ca<sup>2+</sup> and H<sup>+</sup>  
278 concentrations are 0.98 (0.62 – 1.27), 10.40 (8.35 – 16.06), 1.29 (0.87 – 2.13), 0.27 (0.21 – 0.33), 0.24  
279 (0.03 – 0.56), 0.05 (0.03 – 0.08), 0.18 (0.15 – 0.22), 0.18 (0.05 – 0.57) and 11.75 (9.56 – 18.12) µeq L<sup>-1</sup>,  
280 respectively. H<sup>+</sup> and NO<sub>3</sub><sup>-</sup> are the most abundant species, accounting for 46.4 and 41.0 % of the total  
281 ions, followed by SO<sub>4</sub><sup>2-</sup> (5.1 %) and Cl<sup>-</sup> (3.9 %). The other 5 cations, Na<sup>+</sup>, NH<sub>4</sub><sup>+</sup>, K<sup>+</sup>, Mg<sup>2+</sup> and Ca<sup>2+</sup>,  
282 only represent 3.6 % of the total ion budget. A significant linear relationship was found between NO<sub>3</sub><sup>-</sup>  
283 and the total ionic strength ( $R^2 = 0.99$ ,  $p < 0.01$ ), possibly suggesting that NO<sub>3</sub><sup>-</sup> is the species  
284 controlling ion abundance by influencing acidity of the crystal ice (i.e., H<sup>+</sup> levels). In comparison with  
285 surface snow, concentrations of H<sup>+</sup> and NO<sub>3</sub><sup>-</sup> are significantly higher in crystal ice (Independent  
286 Samples T Test,  $p < 0.01$ ), while concentrations of Cl<sup>-</sup>, SO<sub>4</sub><sup>2-</sup>, Na<sup>+</sup>, NH<sub>4</sub><sup>+</sup>, K<sup>+</sup>, Mg<sup>2+</sup> and Ca<sup>2+</sup> are  
287 comparable in the two types of snow samples (Fig. S2 in supporting information). To date, the  
288 information on the chemistry of ice crystal is rather limited but data from the so-called skin layer at  
289 Dome C (top ~4 mm snow), where NO<sub>3</sub><sup>-</sup> concentrations are in the range of 9 – 22 µeq L<sup>-1</sup> in  
290 summertime (Erbland et al., 2013), are generally comparable to our observations.

291 NO<sub>3</sub><sup>-</sup> concentrations in surface snow have been widely measured across Antarctica (Fig. 2), and the  
292 values vary from 0.2 to 12.9 µeq L<sup>-1</sup>, with a mean of 2.1 µeq L<sup>-1</sup> ( $n = 594$ ,  $1\sigma = 1.7$  µeq L<sup>-1</sup>) and a  
293 median of 1.4 µeq L<sup>-1</sup>. Most of the data (87 %) fall in the range of 0.5 - 4.0 µeq L<sup>-1</sup>, and only 7 % of the  
294 values are above 5.0 µeq L<sup>-1</sup>, mainly distributed on the East Antarctic plateaus. Spatially, NO<sub>3</sub><sup>-</sup>  
295 concentrations show an increasing trend with distance inland, and the values are higher in East than in  
296 West Antarctica. Overall, this spatial pattern is opposite to that of the annual snow accumulation rate  
297 (Arthern et al., 2006), i.e., low (high) snow accumulation corresponds to high (low) NO<sub>3</sub><sup>-</sup>  
298 concentrations. It is difficult to compare with NO<sub>3</sub><sup>-</sup> concentrations derived from the “upper snow layer”  
299 in different studies because each study sampled a different depth (Fig. 2), e.g., 2 - 10 cm for  
300 DDU-Dome C traverse (Frey et al., 2009; Erbland et al., 2013), 25 cm for the 1989-1990 International  
301 Trans-Antarctica Expedition (Qin et al., 1992) and 3 cm for this study. The different sampling depths  
302 can result in large differences in NO<sub>3</sub><sup>-</sup> concentration, especially on the East Antarctic plateaus (e.g., the  
303 values of the topmost 1 cm of snow, the crystal ice in this study, can be up to >15 µeq L<sup>-1</sup>; Fig. 1).  
304 Because of this, any comparison of NO<sub>3</sub><sup>-</sup> concentrations in surface snow collected in different  
305 campaigns should be made with caution.

306

### 307 3.2 Snowpit NO<sub>3</sub><sup>-</sup> concentrations

308 Mean NO<sub>3</sub><sup>-</sup> concentrations for snowpits are shown in Fig. 1. From the coast to ~450 km inland,  
309 snowpit NO<sub>3</sub><sup>-</sup> means are comparable to those of surface snow; whereas, NO<sub>3</sub><sup>-</sup> means are lower in inland



310 snowpits than in surface snow with the exception of sites ~800 km from the coast. In general, the  
311 differences between snowpit  $\text{NO}_3^-$  means and the corresponding surface snow values are small at sites  
312 with high snow accumulation (e.g., close to coast), while the differences are large in low snow  
313 accumulation areas (e.g., near Dome A).

314 The profiles of  $\text{NO}_3^-$  for all snowpits are shown in Fig. 3.  $\text{NO}_3^-$  concentrations vary remarkably with  
315 depth in pits SP1 - SP5, which are located near the coast. Although SP2 and SP5 show high  $\text{NO}_3^-$   
316 concentrations in the topmost sample, the data from deeper depths can be compared with the surface  
317 values. In addition,  $\text{NO}_3^-$  means for the entire snowpits are close to the means of the topmost layer  
318 covering a full annual cycle of accumulation (i.e., the most recent year of snow accumulation) at  
319 SP1-SP5 (Fig. 4). Given the high snow accumulation (Fig. 1),  $\text{NO}_3^-$  variability in coastal snowpits is  
320 likely suggestive of a seasonal signature (Wagenbach et al., 1998b; Grannas et al., 2007; Shi et al.,  
321 2015). Among the coastal snowpits, water isotope ratios ( $\delta^{18}\text{O}$  of  $\text{H}_2\text{O}$ ) of samples at SP2 were also  
322 determined, thus allowing for investigating  $\text{NO}_3^-$  seasonal variability (Fig. S3 in supporting  
323 information). In general, the  $\delta^{18}\text{O}(\text{H}_2\text{O})$  peaks correspond to high  $\text{NO}_3^-$  concentrations (i.e.,  $\text{NO}_3^-$  peaks  
324 present in summer). This seasonal pattern is in agreement with previous observations of  $\text{NO}_3^-$  in  
325 snow/ice and atmosphere in coastal Antarctica (Mulvaney and Wolff, 1993; Mulvaney et al., 1998;  
326 Wagenbach et al., 1998b; Savarino et al., 2007).

327 In contrast, most of the inland snowpits show high  $\text{NO}_3^-$  concentrations in the top layer, and then fall  
328 sharply from  $> 2.0 \mu\text{eq L}^{-1}$  in top snow to  $< 0.2 \mu\text{eq L}^{-1}$  in the first meter of depth (Fig. 3).  $\text{NO}_3^-$  means  
329 for the entire snowpits are typically lower than those of the most recent year snow layer (Fig. 4).  
330 Similar  $\text{NO}_3^-$  profiles for snowpits have been reported elsewhere in Antarctica, as a result of  
331 post-depositional processing of  $\text{NO}_3^-$  (R  hlisberger et al., 2000; McCabe et al., 2007; Erbland et al.,  
332 2013; Shi et al., 2015).

333 Comparison of the  $\text{NO}_3^-$  profile patterns reveals significant spatial heterogeneity, even for  
334 neighboring sites. For instance, sites SP11 and SP12, 14 km apart, feature similar snow accumulation  
335 rate (Table 1). If it is assumed that snow accumulation is relatively constant during the past several  
336 years at SP11 (sampled in 2012/2013), snow in the depth of ~54 cm corresponds to the deposition in  
337 2009/2010 (snow density =  $0.45 \text{ g cm}^{-3}$ , from field measurements).  $\text{NO}_3^-$  concentrations are much  
338 higher in the top snow of SP12 (sampled in 2009/2010) than in the depth of ~54 cm in SP11 (Fig. 3).  
339 This variation in  $\text{NO}_3^-$  profiles at a local scale has been reported, possibly related to local morphologies  
340 associated with sastrugi formation and wind drift (Frey et al., 2009; Traversi et al., 2009). It is  
341 interesting that higher  $\text{NO}_3^-$  concentrations were not found in the uppermost layer at sites SP7 and SP8  
342 (~600 km from coast; Fig. 3), where large sastrugi with hard smooth surfaces was extensively  
343 developed (from field observations; Fig. S4 in supporting information). Snow accumulation rate in this  
344 area fluctuates remarkably, and the values of some sites are rather small or close to zero due to the  
345 strong wind scouring (Fig. 1) (Ding et al., 2011; Das et al., 2013). In this case, the snowpit  $\text{NO}_3^-$   
346 profiles appear to be largely influenced by wind scour on snow, possibly resulting in missing years  
347 and/or intra-annual mixing.

348

## 349 **4 Discussion**

350

### 351 **4.1 Accumulation influence on $\text{NO}_3^-$**

352 The preservation of  $\text{NO}_3^-$  is thought to be closely associated with snow accumulation, where most of  
353 the deposited  $\text{NO}_3^-$  is preserved at sites with higher snow accumulation (Wagenbach et al., 1994;

354 Hastings et al., 2004; Fibiger et al., 2013). Whereas  $\text{NO}_3^-$  may be altered significantly at sites with low  
 355 snow accumulation, largely due to photolysis (Blunier et al., 2005; Grannas et al., 2007; Frey et al.,  
 356 2009; Erbland et al., 2013; Erbland et al., 2015). In the following discussion, we divide the traverse  
 357 into two zones, i.e., the coastal zone (<~450 km from the coast, including SP1-SP5 and Core 1; Table 1)  
 358 and the inland region (~450 km to Dome A, including pits SP6-SP20 and Core 2; Table 1), following  
 359  $\text{NO}_3^-$  distribution patterns in surface snow and snowpits (sections 3.1 and 3.2) as well as the spatial  
 360 pattern of snow accumulation rate (Fig. 1).

361 As for snowpits,  $\text{NO}_3^-$  levels in top and deeper layers are comparable near the coast, while  $\text{NO}_3^-$   
 362 differs considerably between the upper and deeper snow at inland sites (Figs. 3 and 4). Photochemical  
 363 processing is responsible for  $\text{NO}_3^-$  distribution in inland snowpits (Erbland et al., 2013; Berhanu et al.,  
 364 2015). Considering that the actinic flux is always negligible below the depth of 1 m, the bottom layers  
 365 of the snowpits (i.e., > 100 cm; Table 1) are well below the photochemically active zone (France et al.,  
 366 2011; Zatkan et al., 2013). In this case,  $\text{NO}_3^-$  in the bottom snowpit, i.e., below the photic zone, can be  
 367 taken as the archived fraction without further modification, as also suggested by previous observations  
 368 (Frey et al., 2009; Erbland et al., 2013; Erbland et al., 2015). Here, we define  $\text{NO}_3^-$  in the bottom layer  
 369 covering a full annual cycle of deposition as an approximation of the annual mean of archived  $\text{NO}_3^-$   
 370 (i.e., beyond photochemical processing; denoted as “ $C_{\text{archived}}$ ” in the following context; Fig. 4), thus  
 371 allowing for calculating the archived annual  $\text{NO}_3^-$  flux (i.e., the product of  $C_{\text{archived}}$  and annual snow  
 372 accumulation rate). Although there is uncertainty in the calculation of archived  $\text{NO}_3^-$  flux due to  
 373 interannual variability in  $\text{NO}_3^-$  inputs and snow accumulation, this assumption provides a useful way to  
 374 investigate the relationship between preservation of  $\text{NO}_3^-$  and physical factors considering that an  
 375 extensive array of ice core measurements is unavailable in most of Antarctica. It is noted that  $C_{\text{archived}}$  is  
 376 generally close to (lower than) the  $\text{NO}_3^-$  means for entire snowpits in coastal (inland) Antarctica (Fig.  
 377 4).

378

#### 379 4.1.1 $\text{NO}_3^-$ in coastal snowpack

380 The simplest plausible model to relate flux and concentration of  $\text{NO}_3^-$  in snow to its atmospheric  
 381 concentration (Legrand, 1987; Alley et al., 1995) can be expressed as,

$$382 F_{\text{total}} = K_1 C_{\text{atm}} + K_2 C_{\text{atm}} A \text{ (Eq. 4),}$$

$$383 F_{\text{total}} = C_{\text{firm}} \times A \text{ (Eq. 5),}$$

384 where  $F_{\text{total}}$  is snow  $\text{NO}_3^-$  flux ( $\mu\text{eq m}^{-2} \text{ a}^{-1}$ );  $C_{\text{atm}}$  is atmospheric concentration of  $\text{NO}_3^-$  ( $\mu\text{eq m}^{-3}$ );  $A$  is  
 385 annual snow accumulation rate ( $\text{kg m}^{-2} \text{ a}^{-1}$ );  $C_{\text{firm}}$  is measured firm  $\text{NO}_3^-$  concentration ( $\mu\text{eq L}^{-1}$ , here  
 386  $C_{\text{firm}} = C_{\text{archived}}$ );  $K_1$  is the dry deposition velocity ( $\text{cm s}^{-1}$ ); and  $K_2$  is the scavenging ratio for precipitation  
 387 ( $\text{m}^3 \text{ kg}^{-1}$ ), which allows conversion of atmospheric concentration to snow concentration of  $\text{NO}_3^-$  in this  
 388 study. From Eqs. 4 and 5, firm  $\text{NO}_3^-$  concentration can be expressed as,

$$389 C_{\text{firm}} = K_1 C_{\text{atm}} \times 1/A + K_2 C_{\text{atm}} \text{ (Eq. 6)}$$

390 If  $K_1$  and  $K_2$  are constants, a linear relationship between measured  $\text{NO}_3^-$  concentration ( $C_{\text{firm}}$ ) and snow  
 391 accumulation ( $A$ ) can be interpreted using Eq. 6, which assumes regional spatial homogeneity of fresh  
 392 snow  $\text{NO}_3^-$  levels and dry deposition flux. The slope ( $K_1 C_{\text{atm}}$ ) of the linear model represents an  
 393 approximation of dry deposition flux of  $\text{NO}_3^-$  (i.e., an apparent dry deposition flux), while the intercept  
 394 ( $K_2 C_{\text{atm}}$ ) stands for  $\text{NO}_3^-$  concentration in fresh snowfall. If dry deposition ( $K_1 C_{\text{atm}}$ ) is much larger than  
 395 wet deposition ( $K_2 C_{\text{atm}} A$ ), the concentration of  $\text{NO}_3^-$  in snow will be proportional to its concentration in  
 396 the atmosphere. In the condition of a constant atmospheric concentration, larger snow accumulation  
 397 will increase the flux of  $\text{NO}_3^-$  but decrease its concentration in snow. While this linear model is a gross

398 over-simplification of the complex nature of air-snow exchange of  $\text{NO}_3^-$ , it provides a simple approach  
399 to compare the processes occurring on the coast versus those inland. In addition, this model can  
400 provide useful parameter values in modeling  $\text{NO}_3^-$  deposition/preservation at large scales, considering  
401 that observations remain sparse across Antarctica (e.g., Zatzko et al., 2016).

402 The relationship between  $C_{\text{archived}}$  of  $\text{NO}_3^-$  and snow accumulation rate is shown in Fig. 5. The linear  
403 fit of  $C_{\text{archived}}$  vs. inverse snow accumulation ( $R^2=0.88$ ,  $p<0.01$ ; Fig. 5a) supports the assumptions of  
404 spatial homogeneity. The intercept and slope of the linear fit suggest a  $\text{NO}_3^-$  concentration in fresh  
405 snow and an apparent  $\text{NO}_3^-$  dry deposition flux of  $0.7\pm 0.07 \mu\text{eq L}^{-1}$  and  $45.7\pm 7.8 \mu\text{eq m}^{-2} \text{a}^{-1}$   
406 respectively. The apparent dry deposition flux is opposite to the observation in Dronning Maud Land  
407 (DML) region, where a negative dry deposition flux suggested net losses of  $\text{NO}_3^-$  (Pasteris et al., 2014).

408 Figure 5b shows the archived fluxes of  $\text{NO}_3^-$  on the coast, with values from 104 (at the lowest  
409 accumulation site) to  $169 \mu\text{eq m}^{-2} \text{a}^{-1}$  (at the highest accumulation site). Taking the calculated  $\text{NO}_3^-$  dry  
410 deposition flux of  $45.7 \mu\text{eq m}^{-2} \text{a}^{-1}$ , dry deposition accounts for 27-44 % (mean = 36 %) of total  $\text{NO}_3^-$   
411 inputs, with higher (lower) percentages at lower (higher) snow accumulation sites. This result is in line  
412 with the observations in Taylor Valley (coastal West Antarctica), where the snowfall was found to be  
413 the primary driver for  $\text{NO}_3^-$  inputs (Witherow et al., 2006). This observation also generally agrees with,  
414 but is greater than that in the modeling study of Zatzko et al. (2016), which predicts a ratio of dry  
415 deposition to total deposition of  $\text{NO}_3^-$  in Antarctica as  $< 20\%$  close to the coast, increasing towards the  
416 plateaus.

417 In Figs. 5a and b, the strong linear relationships between  $\text{NO}_3^-$  and snow accumulation support that  
418  $K_1$  and  $K_2$  are relatively constant on the coast (Eqs. 4 and 6). The average atmospheric concentration of  
419  $\text{NO}_3^-$  in the coastal  $\sim 450$  km region is  $15.6 \text{ ng m}^{-3}$  in summer (Table S1 in supporting information).  
420 Taking  $C_{\text{atm}}=15.6 \text{ ng m}^{-3}$ ,  $K_1$  is estimated to be  $0.6 \text{ cm s}^{-1}$ , close to a typical estimate for  $\text{HNO}_3$   
421 deposition velocity to a snow/ice surface ( $0.5 \text{ cm s}^{-1}$ ; Seinfeld and Pandis, 1997). This predicted  $K_1$   
422 value is lower than that calculated for the dry deposition of  $\text{HNO}_3$  at South Pole ( $0.8 \text{ cm s}^{-1}$ ; Huey et al.,  
423 2004). It is noted that the true  $K_1$  value could be larger than the prediction ( $0.6 \text{ cm s}^{-1}$ ) due to the higher  
424 values of  $C_{\text{atm}}$  in summer (i.e.,  $15.6 \text{ ng m}^{-3}$  for the calculation of  $K_1$ ) than in other seasons (Mulvaney et  
425 al., 1998; Wagenbach et al., 1998b; Savarino et al., 2007). The scavenging ratio for precipitation ( $K_2$ ) is  
426 estimated to be about  $0.2 \times 10^4 \text{ m}^3 \text{ kg}^{-1}$ , i.e.,  $2 \text{ m}^3 \text{ g}^{-1}$ .

427 If it is assumed that  $\text{NO}_3^-$  concentration in snow is related to its concentration in the atmosphere, the  
428 scavenging ratio for  $\text{NO}_3^-$  ( $W$ ) can be calculated on a mass basis from the following expression  
429 (Kasper-Giebl et al., 1999),

$$430 \quad W = \rho_{\text{atm}} \times (C_{\text{f-snow}} / C_{\text{atm}}) \text{ (Eq. 7)},$$

431 where  $\rho_{\text{atm}}$  is air density ( $\text{g m}^{-3}$ ), and  $C_{\text{f-snow}}$  and  $C_{\text{atm}}$  are  $\text{NO}_3^-$  concentrations in fresh snow ( $\text{ng g}^{-1}$ ) and  
432 atmosphere ( $\text{ng m}^{-3}$ ) respectively. If taking  $\rho_{\text{atm}} \approx 1000 \text{ g m}^{-3}$  (on average, ground surface temperature  $t$   
433  $\approx 255 \text{ K}$ , ground pressure  $P \approx 0.08 \text{ MPa}$ , in the coastal region),  $C_{\text{f-snow}} = 43 \text{ ng g}^{-1}$  (see discussion above  
434 and section 4.2 below), and  $C_{\text{atm}} = 15.6 \text{ ng m}^{-3}$ ,  $W$  is calculated to be  $\sim 2700$ , generally comparable to  
435 previous reports (Barrie, 1985; Kasper-Giebl et al., 1999; Shrestha et al., 2002). It is noted that the  
436 calculation here may be subject to uncertainty, due to the complex transfer of atmospheric  $\text{NO}_3^-$  into the  
437 snow. However, the scavenging ratio provides valuable insights into the relation between  $\text{NO}_3^-$   
438 concentrations in the atmosphere and snow, which might be useful in modeling  $\text{NO}_3^-$  deposition at a  
439 large-scale.

440 Figure 5c shows the distribution of flux is negatively correlated with  $C_{\text{archived}}$  of  $\text{NO}_3^-$ , which is not  
441 surprising since  $C_{\text{archived}}$  is positively related to inverse accumulation (Fig. 5a). Based on the observed

442 strong linear relationship between  $\text{NO}_3^-$  flux and snow accumulation (Fig. 5b), the archived  $\text{NO}_3^-$  flux  
443 is more accumulation dependent compared to  $C_{\text{archived}}$ . This is compatible with the observations in  
444 Greenland (Burkhart et al., 2009), where accumulation is generally above  $100 \text{ kg m}^{-2} \text{ a}^{-1}$ , similar to the  
445 coastal values in this study.

446 In terms of surface snow on the coast,  $\text{NO}_3^-$  may be disturbed by the katabatic winds and wind  
447 convergence located near the Amery Ice Shelf (that is, the snow-sourced  $\text{NO}_x$  and  $\text{NO}_3^-$  from the  
448 Antarctic plateau possibly contributes to coastal snow  $\text{NO}_3^-$ ) (Parish and Bromwich, 2007; Ma et al.,  
449 2010; Zatko et al., 2016). In addition, the sampled  $\sim 3 \text{ cm}$  surface layer roughly corresponds to the net  
450 accumulation in the past 0.5-1.5 months assuming an even distribution of snow accumulation in the  
451 course of a single year. This difference in exposure time of the surface snow at different sampling sites,  
452 could possibly affect the concentration of  $\text{NO}_3^-$ , although the post-depositional alteration of  $\text{NO}_3^-$  was  
453 thought to be minor on the coast (Wolff et al., 2008; Erbland et al., 2013; Shi et al., 2015). Taken  
454 together,  $\text{NO}_3^-$  in coastal surface snow might represent some post-depositional alteration. Even so, a  
455 negative correlation between  $\text{NO}_3^-$  concentration and snow accumulation rate was found at the coast  
456 ( $R^2=0.42$ ,  $p<0.01$ ; Fig. 6a), suggesting that overall the majority of the  $\text{NO}_3^-$  appears to be preserved and  
457 is determined by snow accumulation.

458

#### 459 **4.1.2 $\text{NO}_3^-$ in inland snowpack**

460 In comparison with the coast, the correlation between  $C_{\text{archived}}$  and inverse snow accumulation is  
461 relatively weak in inland regions (Fig. 5d), suggesting more variable conditions in ambient  
462 concentrations and dry deposition flux of  $\text{NO}_3^-$ . In addition, the relationship of  $C_{\text{archived}}$  vs. inverse  
463 accumulation inland is opposite to that of coast. Based on current understanding of the  
464 post-depositional processing of  $\text{NO}_3^-$ , the negative correlation between  $C_{\text{archived}}$  and inverse snow  
465 accumulation (Fig. 5d) suggests losses of  $\text{NO}_3^-$ . The slope of the linear relationship indicates apparent  
466  $\text{NO}_3^-$  dry deposition flux of  $-44.5 \pm 13.0 \mu\text{eq m}^{-2} \text{ a}^{-1}$ , much larger than that of DML ( $-22.0 \pm 2.8 \mu\text{eq m}^{-2}$   
467  $\text{a}^{-1}$ ), where the snow accumulation is generally lower than  $100 \text{ kg m}^{-2} \text{ a}^{-1}$  (Pasteris et al., 2014). At  
468 Kohlen Station (an inland site in East Antarctica), with snow accumulation of  $71 \text{ kg m}^{-2} \text{ a}^{-1}$ , the  
469 emission flux of  $\text{NO}_3^-$  is estimated to be  $-22.9 \pm 13.7 \mu\text{eq m}^{-2} \text{ a}^{-1}$  (Weller and Wagenbach, 2007), which  
470 is also smaller in comparison with this observation. Weller et al. (2004) proposed that loss rate of  $\text{NO}_3^-$   
471 does not depend on snow accumulation rate and the losses become insignificant at accumulation rates  
472 above  $100 \text{ kg m}^{-2} \text{ a}^{-1}$ . Among the inland sites, SP10 and Core2 ( $\sim 800 \text{ km}$  from the coast), featured by  
473 high snow accumulation rate ( $> 100 \text{ kg m}^{-2} \text{ a}^{-1}$ ; Table 1 and Fig. 1), exhibit even higher values of  
474  $C_{\text{archived}}$  and archived fluxes of  $\text{NO}_3^-$  than those of the coastal sites. It is noted that these two cases  
475 influence the linear regression significantly (Fig. 5d). If the two sites are excluded, we can get a linear  
476 regression with a slope of  $-27.7 \pm 9.2 \mu\text{eq m}^{-2} \text{ a}^{-1}$ , which is comparable to previous reports in DML  
477 (Pasteris et al., 2014).

478 The depths of inland snowpits cover several to tens of years snow accumulation, thus allowing for  
479 directly investigating  $\text{NO}_3^-$  emission rate. The difference between  $\text{NO}_3^-$  concentrations in the snow  
480 layer accumulated during the most recent year (Fig. 4) and in the snow accumulated during the year  
481 before the most recent year can represent the loss rate of  $\text{NO}_3^-$ . If it is assumed that snow accumulation  
482 rate is relatively constant during recent decades at specific-sites, on average,  $36.7 \pm 21.3 \%$  of  $\text{NO}_3^-$  (in  
483  $\mu\text{eq L}^{-1}$ ) was lost during one year, with the two sites (SP10 and Core2) with snow accumulation  $> 100$   
484  $\text{kg m}^{-2} \text{ a}^{-1}$  excluded from the calculation. The percentages are generally higher at the sites with lower  
485 snow accumulation rate. Together with snow accumulation rate, the emission flux of  $\text{NO}_3^-$  is calculated

486 to be  $-28.1 \pm 23.0 \mu\text{eq m}^{-2} \text{a}^{-1}$ , close to the linear model prediction ( $-27.7 \pm 9.2 \mu\text{eq m}^{-2} \text{a}^{-1}$ ). Significant  
487 losses can account for  $\text{NO}_3^-$  profiles at inland sites, i.e.,  $\text{NO}_3^-$  concentration decreasing with increasing  
488 depths. Previous observations and modeling works suggested that photolysis dominates the losses (Frey  
489 et al., 2009; Erbland et al., 2013; Shi et al., 2015). During photolysis of  $\text{NO}_3^-$ , some of the  
490 photoproducts ( $\text{NO}_x$ ) are emitted into the gas phase (Davis et al., 2004; France et al., 2011), and these  
491 products should undergo reoxidation by the local oxidants (e.g., hydroxyl radical (OH),  $\text{NO}_2 + \text{OH} + \text{M}$   
492  $\rightarrow \text{HNO}_3 + \text{M}$ ), forming gas phase  $\text{HNO}_3$ . In inland Antarctica, the dominant  $\text{NO}_3^-$  species in the  
493 atmosphere is gaseous  $\text{HNO}_3$  during summertime, while particulate  $\text{NO}_3^-$  is more important in winter  
494 (Legrand et al., 2017b; Traversi et al., 2017). The high levels of gas phase  $\text{HNO}_3$  in summer support the  
495 importance of the re-emission from snow through the photolysis of  $\text{NO}_3^-$  in affecting the atmospheric  
496  $\text{NO}_x/\text{NO}_3^-$  budget (Erbland et al., 2013). On the one hand, the gaseous  $\text{HNO}_3$  can be efficiently  
497 co-condensed with water vapour onto the extensively developed crystal ice layers on Antarctic plateaus  
498 (e.g., Fig. S1 in supporting information), leading to an enrichment of  $\text{NO}_3^-$  in surface snow (Bock et al.,  
499 2016). On the other hand, a large concentration of  $\text{HNO}_3$  would enhance its reaction with sea-salt,  
500 leading to elevated particulate  $\text{NO}_3^-$  concentrations (Legrand et al., 2017b). The significant correlation  
501 between  $\text{NO}_3^-$  and  $\text{H}^+$  in inland Antarctic surface snow ( $R^2 = 0.65$ ,  $p < 0.01$ ) seems to support the  
502 importance of atmospheric gas phase  $\text{HNO}_3$  in affecting surface snow  $\text{NO}_3^-$  concentrations, in  
503 particular  $\text{NO}_3^-$  levels in the crystal ice samples (Fig. 1).

504 Several modeling works have been performed to understand  $\text{NO}_3^-$  recycling processes across  
505 Antarctica (e.g., Erbland et al., 2015; Zatko et al., 2016; Bock et al., 2016), however, each employs  
506 different assumptions and large uncertainty remains in quantifying  $\text{NO}_3^-$  recycling and preservation. It  
507 is thought that emission and transport strength are the main factors controlling the recycling of  $\text{NO}_3^-$ ,  
508 while the former is associated with initial  $\text{NO}_3^-$  concentrations, UV and snow optical properties, and the  
509 latter is linked with air mass movement (Wolff et al., 2008; Frey et al., 2009). As a result, snow  
510 accumulation alone is likely insufficient to account for  $\text{NO}_3^-$  variability in surface snow (i.e., no  
511 significant correlation between  $\text{NO}_3^-$  concentration and snow accumulation; Fig. 6b).

512 The archived  $\text{NO}_3^-$  fluxes vary considerably among inland sites, from  $\sim 3$  to  $333 \mu\text{eq m}^{-2} \text{a}^{-1}$ , with  
513 high values generally corresponding to high snow accumulation (Fig. 5e). However, the nearly 1:1  
514 relationship between  $C_{\text{archived}}$  and  $\text{NO}_3^-$  flux (Fig. 5f), suggests that accumulation rate is not the main  
515 driver of the archived  $\text{NO}_3^-$  concentration. In inland Antarctica, the archived  $\text{NO}_3^-$  fraction is largely  
516 influenced by the length of time that  $\text{NO}_3^-$  was exposed to UV radiation (Berhanu et al., 2015), which  
517 decreases exponentially in the snowpack. The  $e$ -folding depth,  $z_e$  value, is thought to be influenced by a  
518 variety of factors, such as co-existent impurities (e.g., black carbon), bulk density and grain size (Zatko  
519 et al., 2013). In addition, the snow albedo is also dependent on snow physical properties (Carmagnola  
520 et al., 2013). Taken together, this suggests that the inland plateau is below a “threshold” of  
521 accumulation rate such that the archived  $\text{NO}_3^-$  flux cannot be explained by snow accumulation rate.

522

#### 523 **4.2 Effects of coexisting ions on $\text{NO}_3^-$**

524 Atmospheric  $\text{NO}_3^-$  in Antarctica is thought to be mainly associated with mid-latitude sources,  
525 re-formed  $\text{NO}_3^-$  driven by snow-sourced photolysis products, and/or stratospheric inputs (Savarino et  
526 al., 2007; Lee et al., 2014; Traversi et al., 2017 and references therein). Although organic nitrates can  
527 play an important role in the atmospheric  $\text{NO}_y$  budget, multi-seasonal measurements of surface snow  
528  $\text{NO}_3^-$  correlate strongly with inorganic  $\text{NO}_y$  species (especially  $\text{HNO}_3$ ) rather than organic (Jones et al.,  
529 2011). Here, we investigate whether  $\text{NO}_3^-$  in snow is closely associated with coexisting ions (e.g.,  $\text{Cl}^-$ ,

530  $\text{SO}_4^{2-}$ ,  $\text{Na}^+$ ,  $\text{K}^+$ ,  $\text{Mg}^{2+}$  and  $\text{Ca}^{2+}$ ) since these ions have different main sources, e.g.,  $\text{Cl}^-$  and  $\text{Na}^+$  are  
531 predominantly influenced by sea salt, and  $\text{SO}_4^{2-}$  is likely dominated by marine inputs (e.g., sea salt and  
532 bio-activity source) (Bertler et al., 2005). In the snow,  $\text{Cl}^-$ ,  $\text{Na}^+$  and  $\text{SO}_4^{2-}$  are the most abundant ions in  
533 addition to  $\text{NO}_3^-$ .

534 In surface snow, the non-sea salt fraction of  $\text{SO}_4^{2-}$  accounted for 75-99 % of its total budget, with a  
535 mean of 95 %. The percentages were relatively higher in inland regions than at coastal sites. On the  
536 coast, a positive relationship was found between  $\text{nssSO}_4^{2-}$  and  $\text{NO}_3^-$  ( $R^2 = 0.32$ ,  $p < 0.01$ ; Fig. 7a).  
537 Previous observations suggest that  $\text{NO}_3^-$  and  $\text{nssSO}_4^{2-}$  peaks in the atmosphere and snow are usually  
538 present in summer (Jourdain and Legrand, 2002; Wolff et al., 2008; Sigl et al., 2016; Legrand et al.,  
539 2017a; Legrand et al., 2017b). However, the similar seasonal pattern of the two species is associated  
540 with distinct sources, i.e.,  $\text{SO}_4^{2-}$  is mainly derived from marine biogenic emissions while  $\text{NO}_3^-$  is  
541 influenced by photolysis and tropospheric transport (Savarino et al., 2007; Lee et al., 2014; Zatzko et al.,  
542 2016). In the atmosphere,  $\text{SO}_4^{2-}$  is typically found on the submicron particles, while most of the  $\text{NO}_3^-$  is  
543 gaseous  $\text{HNO}_3$  and the particulate  $\text{NO}_3^-$  is mainly on intermediate size particles (Jourdain and Legrand,  
544 2002; Rankin and Wolff, 2003; Legrand et al., 2017a; Legrand et al., 2017b). Thus, the correlation  
545 between  $\text{NO}_3^-$  and  $\text{SO}_4^{2-}$  is unlikely explained by the sources or their occurrence state in the atmosphere  
546 (i.e., gaseous and particulate phases). Laluraj et al. (2010) proposed that the correlation between  
547  $\text{nssSO}_4^{2-}$  vs.  $\text{NO}_3^-$  in ice ( $R^2 = 0.31$ ,  $p < 0.01$ ) could be associated with fine  $\text{nssSO}_4^{2-}$  aerosols, which  
548 provide nucleation centers forming multi-ion complexes with  $\text{HNO}_3$  in the atmosphere. This assertion,  
549 however, should be examined further, considering that the complex chemistry of  $\text{SO}_4^{2-}$  and  $\text{NO}_3^-$  in the  
550 atmosphere is far from understood (e.g., Wolff, 1995; Brown et al., 2006). Thus far, the mechanism of  
551  $\text{nssSO}_4^{2-}$  influencing  $\text{NO}_3^-$  in the snowpack, however, is still debated, and it cannot be ruled out that  
552  $\text{nssSO}_4^{2-}$  further affects mobilization of  $\text{NO}_3^-$  during and/or after crystallization (Legrand and Kirchner,  
553 1990; Wolff, 1995; R thlisberger et al., 2000). It is noted that no relationship was found between  
554  $\text{nssSO}_4^{2-}$  and  $\text{NO}_3^-$  in inland snow (Fig. 7d), possibly due to the strong alteration of  $\text{NO}_3^-$  during  
555 post-depositional processes, as discussed in section 4.1.2.

556 In comparison with  $\text{nssSO}_4^{2-}$  aerosols, the sea-salt aerosols ( $\text{Na}^+$ ) are coarser and can be removed  
557 preferentially from the atmosphere due to a larger dry deposition velocity. High atmospheric sea salt  
558 aerosol concentrations are expected to promote the conversion of gaseous  $\text{HNO}_3$  to the particulate  
559 phase, considering that most of the  $\text{NO}_3^-$  in the atmosphere is in the gas phase ( $\text{HNO}_3$ ). In this case,  
560 particulate  $\text{NO}_3^-$  can be efficiently lost via aerosol mechanisms. In addition, the saline ice also favors  
561 the direct uptake of gaseous  $\text{HNO}_3$  to the ice surface. Changes in partitioning between gas phase  
562 ( $\text{HNO}_3$ ) and particulate phase will affect  $\text{NO}_3^-$  levels due to the different wet and dry deposition rates of  
563 the two species (Aw and Kleeman, 2003). Thus, sea salt aerosols play an important role in the  
564 scavenging of gaseous  $\text{HNO}_3$  from the atmosphere (Hara et al., 2005), and elevated  $\text{NO}_3^-$   
565 concentrations are usually accompanied by  $\text{Na}^+$  spikes in the snowpack (e.g., at Halley station; Wolff et  
566 al., 2008). Surprisingly, no significant correlation was found between  $\text{Na}^+$  and  $\text{NO}_3^-$  in coastal snow  
567 (Fig. 7b). The concentration profiles of  $\text{NO}_3^-$  and  $\text{Na}^+$  in coastal surface snow are shown in Fig. 8, and  
568  $\text{NO}_3^-$  roughly corresponds to  $\text{Na}^+$  in some areas, e.g., 50-150 km and 300-450 km distance inland,  
569 although in general they are not very coherent. It is noted that amongst the 4 snow samples with  $\text{Na}^+ >$   
570  $1.5 \mu\text{eq L}^{-1}$  (open circles in Fig. 8), only one sample co-exhibits a  $\text{NO}_3^-$  spike. This is different from  
571 observations at Halley station, where  $\text{Na}^+$  peaks usually led to elevated  $\text{NO}_3^-$  levels in surface snow in  
572 summer (Wolff et al., 2008). Of the 4 largest  $\text{Na}^+$  spikes, one is a fresh snowfall sample (dashed ellipse  
573 in Fig. 8), and this sample shows the highest  $\text{Na}^+$  concentration ( $2.8 \mu\text{eq L}^{-1}$ ) and low  $\text{NO}_3^-$  ( $0.75 \mu\text{eq}$

574 L<sup>-1</sup>). It is noted that NO<sub>3</sub><sup>-</sup> concentration in this fresh snowfall is close to the model predictions  
575 (0.7±0.07 µeq L<sup>-1</sup>; section 4.1.1), validating that the simple linear deposition model (i.e., the Eq. 6) can  
576 well depict the deposition and preservation of NO<sub>3</sub><sup>-</sup> in coastal snowpack. At inland sites, no correlation  
577 was found between NO<sub>3</sub><sup>-</sup> and Na<sup>+</sup> (Fig. 7e), likely explained by the alteration of NO<sub>3</sub><sup>-</sup> concentration by  
578 post-depositional processing.

579 In surface snow, nssCl<sup>-</sup> represents 0-64 % (mean = 40 %) of the total Cl<sup>-</sup>. On the coast, it is of  
580 interest that nssCl<sup>-</sup> in the 4 samples with the highest Na<sup>+</sup> concentrations (open circles in Figs. 7b and 8)  
581 are close to 0, and positive nssCl<sup>-</sup> values were found for the other samples. The fractionation of Na<sup>+</sup> can  
582 occur due to mirabilite precipitation in sea-ice formation at <-8 °C (Marion et al., 1999), possibly  
583 leading to the positive nssCl<sup>-</sup>. However, even if all of SO<sub>4</sub><sup>2-</sup> in sea water is removed via mirabilite  
584 precipitation, only 12 % of sea salt Na<sup>+</sup> is lost (Rankin et al., 2002). Considering the smallest sea ice  
585 extent in summertime in East Antarctica (Holland et al., 2014), the high Cl<sup>-</sup>/Na<sup>+</sup> ratio (mean = 2.1, well  
586 above 1.17 of sea water, in µeq L<sup>-1</sup>) in surface snow is unlikely from sea salt fractionation associated  
587 with mirabilite precipitation in sea-ice formation. In this case, nssCl<sup>-</sup> could be mainly related to the  
588 deposition of volatile HCl, which is from the reaction of H<sub>2</sub>SO<sub>4</sub> and/or HNO<sub>3</sub> with NaCl (Röhrlisberger  
589 et al., 2003). Thus, nssCl<sup>-</sup> in snowpack can roughly represent the atmospherically deposited HCl. In  
590 summertime, most of the dechlorination (i.e., production of HCl) is likely associated with HNO<sub>3</sub> due to  
591 its high atmospheric concentrations (Jourdain and Legrand, 2002; Legrand et al., 2017b). Accordingly,  
592 the observed relationship between NO<sub>3</sub><sup>-</sup> and nssCl<sup>-</sup> (Fig. 7c) appears to suggest that HCl production can  
593 be enhanced by elevated HNO<sub>3</sub> levels in the atmosphere.

594 With regard to the crystal ice, no significant correlation was found between NO<sub>3</sub><sup>-</sup> and the coexisting  
595 ions (e.g., Cl<sup>-</sup>, Na<sup>+</sup> and SO<sub>4</sub><sup>2-</sup>), suggesting that these ions are generally less influential on NO<sub>3</sub><sup>-</sup> in this  
596 uppermost thin layer, compared to the strong air-snow transfer process of NO<sub>3</sub><sup>-</sup> (Erland et al., 2013). It  
597 is noted that NO<sub>3</sub><sup>-</sup> accounts for most of the calculated H<sup>+</sup> concentrations (81-97 %, mean = 89 %), and  
598 a strong linear relationship was found between them ( $R^2 = 0.96, p < 0.01$ ), suggesting that NO<sub>3</sub><sup>-</sup> is mainly  
599 deposited as acid, HNO<sub>3</sub>, rather than in particulate form as salts (e.g., NaNO<sub>3</sub> and Ca(NO<sub>3</sub>)<sub>2</sub>). This  
600 deduction is in line with the atmospheric observations at Dome C, where NO<sub>3</sub><sup>-</sup> was found to be mainly  
601 in gaseous phase (HNO<sub>3</sub>) in summer (Legrand et al., 2017b). On average, the deposition of HNO<sub>3</sub>  
602 contributes > 91 % of NO<sub>3</sub><sup>-</sup> in the crystal ice (the lower limit, 91 %, calculated by assuming all of the  
603 alkaline species (Na<sup>+</sup>, NH<sub>4</sub><sup>+</sup>, K<sup>+</sup>, Mg<sup>2+</sup> and Ca<sup>2+</sup>) are neutralized by HNO<sub>3</sub> in the atmosphere),  
604 suggesting a dominant role of HNO<sub>3</sub> deposition in snow NO<sub>3</sub><sup>-</sup> concentrations. The elevated high  
605 atmospheric NO<sub>3</sub><sup>-</sup> concentrations observed at Dome A (>100 ng m<sup>-3</sup>; 77.12°E and 80.42°S, Table S1 in  
606 supporting information) possibly indicate oxidation of gaseous NO<sub>x</sub> to HNO<sub>3</sub>, providing further  
607 evidence that NO<sub>3</sub><sup>-</sup> recycling driven by photolysis plays an important role in its abundance in snowpack  
608 on East Antarctic plateaus.

609

## 610 5 Conclusions

611 Samples of surface snow, snowpits and the uppermost layer of crystal ice, collected on the traverse  
612 from the coast to Dome A, East Antarctica, were used to investigate the deposition and preservation of  
613 NO<sub>3</sub><sup>-</sup> in snow. In general, a spatial trend of NO<sub>3</sub><sup>-</sup> in surface snow was found on the traverse, with high  
614 (low) concentrations on the plateau (coast). Similarly, NO<sub>3</sub><sup>-</sup> concentrations in the atmosphere are higher  
615 on the plateau than at coastal sites, with a range of 6 to 118 ng m<sup>-3</sup>. Extremely high NO<sub>3</sub><sup>-</sup> levels (e.g., >  
616 10 µeq L<sup>-1</sup>) were observed in the uppermost crystal ice layer, possibly associated with re-deposition of  
617 recycled NO<sub>3</sub><sup>-</sup> from snow-sourced NO<sub>x</sub>. As for the snowpits, NO<sub>3</sub><sup>-</sup> exhibits high levels in the top layer

618 and low concentrations at deeper depths in the inland region, while no clear trend was found on the  
619 coast.

620 On the coast, the archived  $\text{NO}_3^-$  flux in snow is positively correlated with snow accumulation rate,  
621 but negatively with  $\text{NO}_3^-$  concentration. A linear model can well depict the relationship between  
622 archived  $\text{NO}_3^-$  and snow accumulation, supporting that atmospheric levels and dry deposition fluxes of  
623  $\text{NO}_3^-$  are spatially homogeneous on the coast, and that dry deposition plays a minor role in snow  $\text{NO}_3^-$   
624 inputs. The dry deposition velocity and scavenging ratio for  $\text{NO}_3^-$  are estimated to be  $0.5 \text{ cm s}^{-1}$  and  
625 2200, respectively. In inland Antarctica, the archived  $\text{NO}_3^-$  fluxes, varying significantly among sites, are  
626 largely dependent on  $\text{NO}_3^-$  concentration. A weak correlation between snow accumulation and archived  
627  $\text{NO}_3^-$  suggests variable ambient concentrations and dry deposition flux of  $\text{NO}_3^-$ , and the relationship is  
628 opposite to that for the coast. This supports the idea that post-depositional processing dominates  $\text{NO}_3^-$   
629 concentration and distribution in inland Antarctica (e.g., Erbland et al., 2013; Erbland et al., 2015; Shi  
630 et al., 2015; Zatzko et al., 2016).

631 The major ions,  $\text{Cl}^-$ ,  $\text{SO}_4^{2-}$  and  $\text{Na}^+$ , originate from different sources than  $\text{NO}_3^-$ , but could potentially  
632 affect the scavenging and preservation of  $\text{NO}_3^-$ . In coastal surface snow, a positive correlation between  
633  $\text{SO}_4^{2-}$  and  $\text{NO}_3^-$  suggests the potential influence of fine aerosols on  $\text{NO}_3^-$  formation and/or  
634 scavenging, while the coarse sea salt aerosol (e.g.,  $\text{Na}^+$ ) is likely less influential. In contrast to the coast,  
635  $\text{NO}_3^-$  in inland surface snow is dominated by post-depositional processes, and the effects of coexisting  
636 ions on  $\text{NO}_3^-$  appear to be rather minor. In inland surface snow, the strong relationship between  $\text{NO}_3^-$   
637 and  $\text{H}^+$  suggests a dominant role of gaseous  $\text{HNO}_3$  deposition in determining  $\text{NO}_3^-$  concentrations.

638

#### 639 **Associated content**

640 Please see the file of Supporting Information.

641

#### 642 **Data availability**

643 Data on nitrate concentrations in snow on the traverse from coast (Zhongshan Station) to Dome A are  
644 available in the Chinese National Arctic and Antarctic Data Center,

645 <http://www.chinare.org.cn/difDetailPublic/?id=9401>, DOI: 10.11856/SNS.D.2018.001.v0.

646

#### 647 **Competing interests**

648 The authors declare that they have no conflict of interest.

649

#### 650 **Acknowledgement**

651 This project was supported by the National Science Foundation of China (Grant nos. 41576190 and  
652 41206188 to GS, 41476169 to SJ), the National Key Research and Development Program of China  
653 (Grant no. 2016YFA0302204), the Fundamental Research Funds for the Central Universities (Grant No  
654 40500-20101-222006), and Chinese Polar Environment Comprehensive Investigation and Assessment  
655 Programmes (Grant nos. CHINARE 201X-02-02 and 201X-04-01). The authors appreciate the  
656 CHINARE inland members for providing help during sampling. The authors would like to thank Prof.  
657 Joel Savarino and two anonymous referees for their help in the development and improvement of this  
658 paper.

659

#### 660 **References**

661 Alexander, B., Savarino, J., Kreutz, K.J., and Thiemens, M.: Impact of preindustrial biomass-burning



662 emissions on the oxidation pathways of tropospheric sulfur and nitrogen, *J. Geophys. Res.*, 109,  
663 D08303, doi:10.1029/2003JD004218, 2004.

664 Alley, R., Finkel, R., Nishizumi, K., Anandakrishnan, A., Shuman, C., Mershon, G., Zielinski, G., and  
665 Mayewski, P.A.: Changes in continental and sea-salt atmospheric loadings in central Greenland during  
666 the most recent deglaciation: Model-based estimates, *J. Glaciol.*, 41, 503-514, 1995.

667 Arthern, R.J., Winebrenner, D.P., and Vaughan, D.G.: Antarctic snow accumulation mapped using  
668 polarization of 4.3-cm wavelength microwave emission, *J. Geophys. Res.*, 111,  
669 doi:10.1029/2004JD005667, 2006.

670 Aw, J., and Kleeman, M.J.: Evaluating the first-order effect of intraannual temperature variability on  
671 urban air pollution, *J. Geophys. Res.*, 108, -, 2003.

672 Barrie, L.A.: Scavenging ratios, wet deposition, and in-cloud oxidation: An application to the oxides of  
673 sulphur and nitrogen, *J. Geophys. Res.*, 90, 5789–5799, 1985.

674 Berhanu, T.A., Meusinger, C., Erbland, J., Jost, R., Bhattacharya, S., Johnson, M.S., and Savarino, J.:  
675 Laboratory study of nitrate photolysis in Antarctic snow. II. Isotopic effects and wavelength  
676 dependence, *J. Chem. Phys.*, 140, 244306, doi:10.1063/1.4882899, 2014.

677 Berhanu, T.A., Savarino, J., Erbland, J., Vicars, W.C., Preunkert, S., Martins, J.F., and Johnson, M.S.:  
678 Isotopic effects of nitrate photochemistry in snow: a field study at Dome C, Antarctica, *Atmos. Chem.*  
679 *Phys.*, 15, 11243-11256, doi:10.5194/acp-15-11243-2015, 2015.

680 Bertler, N., Mayewski, P.A., Aristarain, A., Barrett, P., Becagli, S., Bernardo, R., Bo, S., Xiao, C., Curran,  
681 M., and Qin, D.: Snow chemistry across Antarctica, *Ann. Glaciol.*, 41, 167-179, 2005.

682 Blunier, T., Floch, G., Jacobi, H.-W., and Quansah, E.: Isotopic view on nitrate loss in Antarctic surface  
683 snow, *Geophys. Res. Lett.*, 32, L13501, doi:10.1029/2005GL023011, 2005.

684 Bock, J., Savarino, J., and Picard, G.: Air–snow exchange of nitrate: a modelling approach to investigate  
685 physicochemical processes in surface snow at Dome C, Antarctica, *Atmos. Chem. Phys.*, 16,  
686 12531-12550, doi:10.5194/acp-16-12531-2016, 2016.

687 Brown, S., Ryerson, T., Wollny, A., Brock, C., Peltier, R., Sullivan, A., Weber, R., Dube, W., Trainer, M.,  
688 and Meagher, J.: Variability in nocturnal nitrogen oxide processing and its role in regional air quality,  
689 *Science*, 311, 67-70, doi:10.1126/science.1120120, 2006.

690 Burkhart, J.F., Bales, R.C., McConnell, J.R., Hutterli, M.A., and Frey, M.M.: Geographic variability of  
691 nitrate deposition and preservation over the Greenland Ice Sheet, *J. Geophys. Res.*, 114,  
692 doi:10.1029/2008JD010600, 2009.

693 Carmagnola, C., Domine, F., Dumont, M., Wright, P., Strellis, B., Bergin, M., Dibb, J., Picard, G., and  
694 Morin, S.: Snow spectral albedo at Summit, Greenland: measurements and numerical simulations  
695 based on physical and chemical properties of the snowpack, *The Cryosphere*, 7, 1139-1160,  
696 doi:10.5194/tc-7-1139-2013, 2013.

697 Das, I., Bell, R.E., Scambos, T.A., Wolovick, M., Creyts, T.T., Studinger, M., Frearson, N., Nicolas, J.P.,  
698 Lenaerts, J.T., and van den Broeke, M.R.: Influence of persistent wind scour on the surface mass  
699 balance of Antarctica, *Nat. Geosci.*, 6, 367-371, doi:10.1038/NGEO1766, 2013.

700 Davis, D., Chen, G., Buhr, M., Crawford, J., Lenschow, D., Lefer, B., Shetter, R., Eisele, F., Mauldin, L., and  
701 Hogan, A.: South Pole NO<sub>x</sub> chemistry: an assessment of factors controlling variability and absolute  
702 levels, *Atmos. Environ.*, 38, 5375-5388, doi:10.1016/j.atmosenv.2004.04.039, 2004.

703 Dibb, J.E., Gregory Huey, L., Slusher, D.L., and Tanner, D.J.: Soluble reactive nitrogen oxides at South  
704 Pole during ISCAT 2000, *Atmos. Environ.*, 38, 5399-5409, doi:10.1016/j.atmosenv.2003.01.001, 2004.

705 Ding, M., Xiao, C., Jin, B., Ren, J., Qin, D., and Sun, W.: Distribution of  $\delta^{18}\text{O}$  in surface snow along a

706 transect from Zhongshan Station to Dome A, East Antarctica, *Chin. Sci. Bull.*, 55, 2709-2714,  
707 doi:10.1007/s11434-010-3179-3, 2010.

708 Ding, M., Xiao, C., Li, Y., Ren, J., Hou, S., Jin, B., and Sun, B.: Spatial variability of surface mass balance  
709 along a traverse route from Zhongshan station to Dome A, Antarctica, *J. Glaciol.*, 57, 658-666, 2011.

710 Duderstadt, K.A., Dibb, J.E., Jackman, C.H., Randall, C.E., Solomon, S.C., Mills, M.J., Schwadron, N.A.,  
711 and Spence, H.E.: Nitrate deposition to surface snow at Summit, Greenland, following the 9 November  
712 2000 solar proton event, *J. Geophys. Res.*, 119, 6938-6957, 2014.

713 Duderstadt, K.A., Dibb, J.E., Schwadron, N.A., Spence, H.E., Solomon, S.C., Yudin, V.A., Jackman, C.H.,  
714 and Randall, C.E.: Nitrate ion spikes in ice cores not suitable as proxies for solar proton events, *J.*  
715 *Geophys. Res.*, 121, 2994-3016, doi:10.1002/2015JD023805, 2016.

716 Erbland, J., Savarino, J., Morin, S., France, J.L., Frey, M.M., and King, M.D.: Air-snow transfer of nitrate  
717 on the East Antarctic plateau -Part 2: An isotopic model for the interpretation of deep ice-core records,  
718 *Atmos. Chem. Phys.*, 15, 12079-12113, doi:10.5194/acp-15-12079-2015, 2015.

719 Erbland, J., Vicars, W., Savarino, J., Morin, S., Frey, M., Frosini, D., Vince, E., and Martins, J.: Air-snow  
720 transfer of nitrate on the East Antarctic Plateau - Part 1: Isotopic evidence for a photolytically driven  
721 dynamic equilibrium in summer, *Atmos. Chem. Phys.*, 13, 6403-6419, doi:10.5194/acp-13-6403-2013,  
722 2013.

723 Felix, J.D., and Elliott, E.M.: The agricultural history of human - nitrogen interactions as recorded in ice  
724 core  $\delta^{15}N - NO_3^-$ , *Geophys. Res. Lett.*, 40, 1642-1646, doi:10.1002/grl.50209, 2013.

725 Fibiger, D.L., Hastings, M.G., Dibb, J.E., and Huey, L.G.: The preservation of atmospheric nitrate in snow  
726 at Summit, Greenland, *Geophys. Res. Lett.*, 40, 3484-3489, doi:10.1002/grl.50659, 2013.

727 France, J., King, M., Frey, M., Erbland, J., Picard, G., Preunkert, S., MacArthur, A., and Savarino, J.: Snow  
728 optical properties at Dome C (Concordia), Antarctica; implications for snow emissions and snow  
729 chemistry of reactive nitrogen, *Atmos. Chem. Phys.*, 11, 9787-9801, doi:10.5194/acp-11-9787-2011,  
730 2011.

731 Frey, M.M., Savarino, J., Morin, S., Erbland, J., and Martins, J.: Photolysis imprint in the nitrate stable  
732 isotope signal in snow and atmosphere of East Antarctica and implications for reactive nitrogen cycling,  
733 *Atmos. Chem. Phys.*, 9, 8681-8696, 2009.

734 Geng, L., Alexander, B., Cole-Dai, J., Steig, E.J., Savarino, J., Sofen, E.D., and Schauer, A.J.: Nitrogen  
735 isotopes in ice core nitrate linked to anthropogenic atmospheric acidity change, *Proc. Natl. Acad. Sci.*,  
736 111, 5808-5812, doi:10.1073/pnas.1319441111, 2014.

737 Geng, L., Murray, L.T., Mickley, L.J., Lin, P., Fu, Q., Schauer, A.J., and Alexander, B.: Isotopic evidence of  
738 multiple controls on atmospheric oxidants over climate transitions, *Nature*, 546, 133-136,  
739 doi:10.1038/nature22340, 2017.

740 Goodwin, I., De Angelis, M., Pook, M., and Young, N.: Snow accumulation variability in Wilkes Land,  
741 East Antarctica, and the relationship to atmospheric ridging in the 130°-170° E region since 1930, *J.*  
742 *Geophys. Res.*, 108, doi:10.1029/2002JD002995 2003.

743 Grannas, A., Jones, A.E., Dibb, J., Ammann, M., Anastasio, C., Beine, H., Bergin, M., Bottenheim, J.,  
744 Boxe, C., and Carver, G.: An overview of snow photochemistry: evidence, mechanisms and impacts,  
745 *Atmos. Chem. Phys.*, 7, 4329-4373, 2007.

746 Hara, K., Osada, K., Kido, M., Matsunaga, K., Iwasaka, Y., Hashida, G., and Yamanouchi, T.: Variations of  
747 constituents of individual sea-salt particles at Syowa station, Antarctica, *Tellus B*, 57, 230-246, 2005.

748 Hastings, M.G., Jarvis, J.C., and Steig, E.J.: Anthropogenic impacts on nitrogen isotopes of ice-core  
749 nitrate, *Science*, 324, 1288-1288, doi:10.1126/science.1170510, 2009.

750 Hastings, M.G., Steig, E., and Sigman, D.: Seasonal variations in N and O isotopes of nitrate in snow at  
751 Summit, Greenland: Implications for the study of nitrate in snow and ice cores, *J. Geophys. Res.*, 109,  
752 D20306, doi:10.1029/2004JD004991, 2004.

753 Holland, P.R., Bruneau, N., Enright, C., Losch, M., Kurtz, N.T., and Kwok, R.: Modeled Trends in Antarctic  
754 Sea Ice Thickness, *J. Climate*, 27, 3784-3801, doi:10.1175/JCLI-D-13-00301.1, 2014.

755 Hou, S., Li, Y., Xiao, C., and Ren, J.: Recent accumulation rate at Dome A, Antarctica, *Chin. Sci. Bull.*, 52,  
756 428-431, 2007.

757 Huey, L.G., Tanner, D.J., Slusher, D.L., Dibb, J.E., Arimoto, R., Chen, G., Davis, D., Buhr, M.P., Nowak, J.B.,  
758 Mauldin Iii, R.L., Eisele, F.L., and Kosciuch, E.: CIMS measurements of HNO<sub>3</sub> and SO<sub>2</sub> at the South Pole  
759 during ISCAT 2000, *Atmos. Environ.*, 38, 5411-5421, doi:10.1016/j.atmosenv.2004.04.037, 2004.

760 Jones, A.E., Weller, R., Minikin, A., Wolff, E.W., Sturges, W.T., McIntyre, H.P., Leonard, S.R., Schrems, O.,  
761 and Bauguitte, S.: Oxidized nitrogen chemistry and speciation in the Antarctic troposphere, *J. Geophys.*  
762 *Res.*, 1042, 21355-21366, 1999.

763 Jones, A.E., Wolff, E.W., Ames, D., Bauguitte, S.-B., Clemmitshaw, K., Fleming, Z., Mills, G., Saiz-Lopez, A.,  
764 Salmon, R.A., and Sturges, W.: The multi-seasonal NO<sub>y</sub> budget in coastal Antarctica and its link with  
765 surface snow and ice core nitrate: results from the CHABLIS campaign, *Atmos. Chem. Phys.*, 11,  
766 9271-9285, 2011.

767 Jourdain, B., and Legrand, M.: Year - round records of bulk and size - segregated aerosol composition  
768 and HCl and HNO<sub>3</sub> levels in the Dumont d'Urville (coastal Antarctica) atmosphere: Implications for  
769 sea - salt aerosol fractionation in the winter and summer, *J. Geophys. Res.*, 107, ACH 20-21 – ACH  
770 20-13, doi:10.1029/2002JD002471, 2002.

771 Kasper-Giebl, A., Kalina, M.F., and Puxbaum, H.: Scavenging ratios for sulfate, ammonium and nitrate  
772 determined at Mt. Sonnblick (3106m a.s.l.), *Atmos. Environ.*, 33, 895-906, 1999.

773 Laluraj, C., Thamban, M., Naik, S., Redkar, B., Chaturvedi, A., and Ravindra, R.: Nitrate records of a  
774 shallow ice core from East Antarctica: Atmospheric processes, preservation and climatic implications,  
775 *The Holocene*, 21, 351-356, doi:10.1177/0959683610374886, 2010.

776 Lee, H.-M., Henze, D.K., Alexander, B., and Murray, L.T.: Investigating the sensitivity of surface-level  
777 nitrate seasonality in Antarctica to primary sources using a global model, *Atmos. Environ.*, 89, 757-767,  
778 doi:10.1016/j.atmosenv.2014.03.003, 2014.

779 Legrand, M.: Chemistry of Antarctic snow and ice, *Le Journal De Physique Colloques*, 48, C1-77-C71-86,  
780 1987.

781 Legrand, M., and Kirchner, S.: Origins and variations of nitrate in South Polar precipitation, *J. Geophys.*  
782 *Res.*, 95, 3493-3507 1990.

783 Legrand, M., and Mayewski, P.A.: Glaciochemistry of polar ice cores: a review, *Rev. Geophys.*, 35,  
784 219-243, 1997.

785 Legrand, M., Preunkert, S., Weller, R., Zipf, L., Elsässer, C., Merchel, S., Rugel, G., and Wagenbach, D.:  
786 Year-round record of bulk and size-segregated aerosol composition in central Antarctica (Concordia  
787 site) – Part 2: Biogenic sulfur (sulfate and methanesulfonate) aerosol, *Atmos. Chem. Phys.*, 17,  
788 14055-14073, doi:10.5194/acp-17-14055-2017, 2017a.

789 Legrand, M., Preunkert, S., Wolff, E., Weller, R., Jourdain, B., and Wagenbach, D.: Year-round records of  
790 bulk and size-segregated aerosol composition in central Antarctica (Concordia site) – Part 1:  
791 Fractionation of sea-salt particles, *Atmos. Chem. Phys.*, 17, 14039-14054,  
792 doi:10.5194/acp-17-14039-2017, 2017b.

793 Legrand, M., Wolff, E., and Wagenbach, D.: Antarctic aerosol and snowfall chemistry: implications for

794 deep Antarctic ice-core chemistry, *Ann. Glaciol.*, 29, 66-72, 1999.

795 Legrand, M.R., Stordal, F., Isaksen, I.S.A., and Rognerud, B.: A model study of the stratospheric budget  
796 of odd nitrogen, including effects of solar cycle variations, *Tellus Series B-chemical & Physical*  
797 *Meteorology*, 41B, 413–426, doi:10.1111/j.1600- 0889.1989.tb00318.x, 1989.

798 Li, C., Ren, J., Qin, D., Xiao, C., Hou, S., Li, Y., and Ding, M.: Factors controlling the nitrate in the DT-401  
799 ice core in eastern Antarctica, *Sci. China Ser. D*, doi:10.1007/s11430-012-4557-2, 2013.

800 Li, Y., Cole-Dai, J., and Zhou, L.: Glaciochemical evidence in an East Antarctica ice core of a recent (AD  
801 1450-1850) neoglacial episode, *J. Geophys. Res.*, 114, doi:10.1029/2008JD011091, 2009.

802 Li, Z., Zhang, M., Qin, D., Xiao, C., Tian, L., Kang, J., and Li, J.: The seasonal variations of  $\delta^{18}\text{O}$ ,  $\text{Cl}^-$ ,  $\text{Na}^+$ ,  
803  $\text{NO}_3^-$  and  $\text{Ca}^{2+}$  in the snow and firn recovered from Princess Elizabeth Land, Antarctica, *Chin. Sci. Bull.*,  
804 44, 2270-2273, 1999.

805 Liss, P.S., Chuck, A.L., Turner, S.M., and Watson, A.J.: Air-sea gas exchange in Antarctic waters, *Antarct.*  
806 *Sci.*, 16, 517-529, doi:10.1017/S0954102004002299, 2004.

807 Ma, Y., Bian, L., Xiao, C., Allison, I., and Zhou, X.: Near surface climate of the traverse route from  
808 Zhongshan Station to Dome A, East Antarctica, *Antarct. Sci.*, 22, 443-459,  
809 doi:10.1017/S0954102010000209, 2010.

810 Marion, G., Farren, R., and Komrowski, A.: Alternative pathways for seawater freezing, *Cold Reg. Sci.*  
811 *Technol.*, 29, 259-266, 1999.

812 Mayewski, P.A., and Legrand, M.R.: Recent increase in nitrate concentration of Antarctic snow, *Nature*,  
813 346, 258-260, 1990.

814 McCabe, J.R., Thiemens, M.H., and Savarino, J.: A record of ozone variability in South Pole Antarctic  
815 snow: Role of nitrate oxygen isotopes, *J. Geophys. Res.*, 112, D12303, doi:10.1029/2006JD007822,  
816 2007.

817 Mulvaney, R., Wagenbach, D., and Wolff, E.W.: Postdepositional change in snowpack nitrate from  
818 observation of year-round near-surface snow in coastal Antarctica, *J. Geophys. Res.*, 103, 11021-11031,  
819 1998.

820 Mulvaney, R., and Wolff, E.: Evidence for winter/spring denitrification of the stratosphere in the nitrate  
821 record of Antarctic firn cores, *J. Geophys. Res.*, 98, 5213-5220, 1993.

822 Mulvaney, R., and Wolff, E.: Spatial variability of the major chemistry of the Antarctic ice sheet, *Ann.*  
823 *Glaciol.*, 20, 440-447, 1994.

824 Parish, T.R., and Bromwich, D.H.: Reexamination of the near-surface airflow over the Antarctic  
825 continent and implications on atmospheric circulations at high southern latitudes, *Mon. Weather. Rev.*,  
826 135, 1961-1973, doi:10.1175/MWR3374.1, 2007.

827 Pasteris, D., McConnell, J.R., Edwards, R., Isaksson, E., and Albert, M.R.: Acidity decline in Antarctic ice  
828 cores during the Little Ice Age linked to changes in atmospheric nitrate and sea salt concentrations, *J.*  
829 *Geophys. Res.*, 119, 5640-5652, doi:10.1002/2013JD020377, 2014.

830 Piel, C., Weller, R., Huke, M., and Wagenbach, D.: Atmospheric methane sulfonate and non-sea-salt  
831 sulfate records at the European Project for Ice Coring in Antarctica (EPICA) deep-drilling site in  
832 Dronning Maud Land, Antarctica, *J. Geophys. Res.*, 111, -, 2006.

833 Qin, D., Zeller, E.J., and Dreschhoff, G.A.: The distribution of nitrate content in the surface snow of the  
834 Antarctic Ice Sheet along the route of the 1990 International Trans-Antarctica Expedition, *J. Geophys.*  
835 *Res.*, 97, 6277-6284, 1992.

836 Röthlisberger, R., Hutterli, M.A., Sommer, S., Wolff, E.W., and Mulvaney, R.: Factors controlling nitrate  
837 in ice cores: Evidence from the Dome C deep ice core, *J. Geophys. Res.*, 105, 20565-20572, 2000.

838 Röthlisberger, R., Hutterli, M.A., Wolff, E.W., Mulvaney, R., Fischer, H., Bigler, M., Goto-Azuma, K.,  
839 Hansson, M.E., Ruth, U., and Siggaard-Andersen, M.-L.: Nitrate in Greenland and Antarctic ice cores: A  
840 detailed description of post-depositional processes, *Ann. Glaciol.*, 35, 209-216, 2002.

841 Röthlisberger, R., Mulvaney, R., Wolff, E.W., Hutterli, M.A., Bigler, M., De Angelis, M., Hansson, M.E.,  
842 Steffensen, J.P., and Udisti, R.: Limited dechlorination of sea-salt aerosols during the last glacial period:  
843 Evidence from the European Project for Ice Coring in Antarctica (EPICA) Dome C ice core, *J. Geophys.*  
844 *Res.*, 108, 4526, doi:4510.1029/2003JD003604, 2003.

845 Rankin, A.M., and Wolff, E.W.: A year-long record of size-segregated aerosol composition at Halley,  
846 Antarctica, *J. Geophys. Res.*, 108, -, 2003.

847 Rankin, A.M., Wolff, E.W., and Martin, S.: Frost flowers: Implications for tropospheric chemistry and ice  
848 core interpretation, *J. Geophys. Res.*, 107, AAC 4-1–AAC 4-15, 2002.

849 Russell, A., McGregor, G., and Marshall, G.: 340 years of atmospheric circulation characteristics  
850 reconstructed from an eastern Antarctic Peninsula ice core, *Geophys. Res. Lett.*, 33, L08702,  
851 doi:08710.01029/02006GL025899, 2006.

852 Russell, A., Mcgregor, G.R., and Marshall, G.J.: An examination of the precipitation delivery  
853 mechanisms for Dolleman Island, eastern Antarctic Peninsula, *Tellus Series A-dynamic Meteorology &*  
854 *Oceanography*, 56, 501–513, 2004.

855 Savarino, J., Kaiser, J., Morin, S., Sigman, D.M., and Thiemens, M.H.: Nitrogen and oxygen isotopic  
856 constraints on the origin of atmospheric nitrate in coastal Antarctica, *Atmos. Chem. Phys.*, 7,  
857 1925-1945, 2007.

858 Seinfeld, J.H., and Pandis, S.N., 1997. *Atmospheric Chemistry and Physics: From Air Pollution to*  
859 *Climate Change*, 2nd ed. Wiley, New York.

860 Shi, G., Buffen, A.M., Hastings, M.G., Li, C., Ma, H., Li, Y., Sun, B., An, C., and Jiang, S.: Investigation of  
861 post-depositional processing of nitrate in East Antarctic snow: isotopic constraints on photolytic loss,  
862 re-oxidation, and source inputs, *Atmos. Chem. Phys.*, 15, 9435–9453, doi:10.5194/acp-15-9435-2015,  
863 2015.

864 Shi, G., Li, Y., Jiang, S., An, C., Ma, H., Sun, B., and Wang, Y.: Large-scale spatial variability of major ions  
865 in the atmospheric wet deposition along the China Antarctica transect (31° N~ 69° S), *Tellus B*, 64,  
866 17134, doi:10.3402/tellusb.v64i0.17134, 2012.

867 Shrestha, A., Wake, C., Dibb, J., and Whitlow, S.: Aerosol and Precipitation Chemistry at a Remote  
868 Himalayan Site in Nepal, *Aerosol Science & Technology*, 36, 441-456, 2002.

869 Sigl, M., Fudge, T.J., Winstrup, M., Coledai, J., Ferris, D., Mcconnell, J.R., Taylor, K.C., Welten, K.C.,  
870 Woodruff, T.E., and Adolphi, F.: The WAIS Divide deep ice core WD2014 chronology - Part 2:  
871 Annual-layer counting (0-31 ka BP), *Clim. Past*, 11, 3425-3474, 2016.

872 Smart, D.F., Shea, M.A., Melott, A.L., and Laird, C.M.: Low time resolution analysis of polar ice cores  
873 cannot detect impulsive nitrate events, *Journal of Geophysical Research: Space Physics*, 119,  
874 9430-9440, doi:10.1002/2014JA020378, 2014.

875 Traversi, R., Becagli, S., Brogioni, M., Caiazzo, L., Ciardini, V., Giardi, F., Legrand, M., Macelloni, G.,  
876 Petkov, B., Preunkert, S., Scarchilli, C., Severi, M., Vitale, V., and Udisti, R.: Multi-year record of  
877 atmospheric and snow surface nitrate in the central Antarctic plateau, *Chemosphere*, 172, 341-354,  
878 doi:10.1016/j.chemosphere.2016.12.143, 2017.

879 Traversi, R., Becagli, S., Castellano, E., Cerri, O., Morganti, A., Severi, M., and Udisti, R.: Study of Dome  
880 C site (East Antarctica) variability by comparing chemical stratigraphies, *Microchem. J.*, 92, 7-14,  
881 doi:10.1016/j.microc.2008.08.007, 2009.

882 Traversi, R., Udisti, R., Frosini, D., Becagli, S., Ciardini, V., Funke, B., Lanconelli, C., Petkov, B., Scarchilli,  
883 C., and Severi, M.: Insights on nitrate sources at Dome C (East Antarctic Plateau) from multi-year  
884 aerosol and snow records, *Tellus B*, 66, 22550, doi:10.3402/tellusb.v66.22550, 2014.

885 Traversi, R., Usoskin, I., Solanki, S., Becagli, S., Frezzotti, M., Severi, M., Stenni, B., and Udisti, R.:  
886 Nitrate in Polar Ice: A New Tracer of Solar Variability, *Sol. Phys.*, 280, 237-254, 2012.

887 Udisti, R., Becagli, S., Benassai, S., Castellano, E., Fattori, I., Innocenti, M., Migliori, A., and Traversi, R.:  
888 Atmospheresnow interaction by a comparison between aerosol and uppermost snow-layers  
889 composition at Dome C, East Antarctica, *Ann. Glaciol.*, 39, 53-61, 2004.

890 Wagenbach, D., Ducroz, F., Mulvaney, R., Keck, L., Minikin, A., Legrand, M., Hall, J.S., and Wolff, E.W.:  
891 Sea-salt aerosol in coastal Antarctic regions, *J. Geophys. Res.*, 103, 10961-10974, 1998a.

892 Wagenbach, D., Graf, V., Minikin, A., Trefzer, U., Kipfstuhl, J., Oerter, H., and Blindow, N.:  
893 Reconnaissance of chemical and isotopic firn properties on top of Berkner Island, Antarctica, *Ann.*  
894 *Glaciol.*, 20, 307-312, 1994.

895 Wagenbach, D., Legrand, M., Fischer, H., Pichlmayer, F., and Wolff, E.W.: Atmospheric near-surface  
896 nitrate at coastal Antarctic sites, *J. Geophys. Res.*, 103, 11007-11020, 1998b.

897 Warren, S.G., Brandt, R.E., and Grenfell, T.C.: Visible and near-ultraviolet absorption spectrum of ice  
898 from transmission of solar radiation into snow, *Appl. Optics*, 45, 5320-5334, 2006.

899 Weller, R., Traufetter, F., Fischer, H., Oerter, H., Piel, C., and Miller, H.: Postdepositional losses of  
900 methane sulfonate, nitrate, and chloride at the European Project for Ice Coring in Antarctica  
901 deep-drilling site in Dronning Maud Land, Antarctica, *J. Geophys. Res.*, 109, 1-9,  
902 doi:10.1029/2003JD004189, 2004.

903 Weller, R., and Wagenbach, D., 2007. Year-round chemical aerosol records in continental Antarctica  
904 obtained by automatic samplings.

905 Witherow, R.A., Lyons, W.B., Bertler, N.A., Welch, K.A., Mayewski, P.A., Sneed, S.B., Nylén, T., Handley,  
906 M.J., and Fountain, A.: The aeolian flux of calcium, chloride and nitrate to the McMurdo Dry Valleys  
907 landscape: evidence from snow pit analysis, *Antarct. Sci.*, 18, 497-505,  
908 doi:10.1017/S095410200600054X, 2006.

909 Wolff, E.W., 1995. Nitrate in polar ice, in: Delmas, R.J. (Ed.), in *Ice core studies of global*  
910 *biogeochemical cycles*. Springer, New York, pp. 195-224.

911 Wolff, E.W., Barbante, S., Becagle, S., Bigler, M., Boutron, C.F., Castellano, E., de Angelis, M., and  
912 Federer, U.: Changes in environment over the last 800,000 years from chemical analysis of the EPICA  
913 Dome C ice core, *Quaternary Sci. Rev.*, 29, 285-295, 2010.

914 Wolff, E.W., Bigler, M., Curran, M., Dibb, J., Frey, M., Legrand, M., and McConnell, J.: The Carrington  
915 event not observed in most ice core nitrate records, *Geophys. Res. Lett.*, 39, L08503,  
916 doi:10.1029/2012GL051603, 2012.

917 Wolff, E.W., Bigler, M., Curran, M.A.J., Dibb, J.E., Frey, M.M., Legrand, M., and McConnell, J.R.:  
918 Comment on "Low time resolution analysis of polar ice cores cannot detect impulsive nitrate events"  
919 by D.F. Smart et al, *J. Geophys. Res.*, 121, 1920-1924, 2016.

920 Wolff, E.W., Jones, A.E., Bauguitte, S.-B., and Salmon, R.A.: The interpretation of spikes and trends in  
921 concentration of nitrate in polar ice cores, based on evidence from snow and atmospheric  
922 measurements, *Atmos. Chem. Phys.*, 8, 5627-5634, 2008.

923 Xiao, C., Mayewski, P.A., Qin, D., Li, Z., Zhang, M., and Yan, Y.: Sea level pressure variability over the  
924 southern Indian Ocean inferred from a glaciochemical record in Princess Elizabeth Land, east  
925 Antarctica, *J. Geophys. Res.*, 109, doi:10.1029/2003JD004065, 2004.

926 Zatzko, M., Grenfell, T., Alexander, B., Doherty, S., Thomas, J., and Yang, X.: The influence of snow grain  
927 size and impurities on the vertical profiles of actinic flux and associated NO<sub>x</sub> emissions on the  
928 Antarctic and Greenland ice sheets, *Atmos. Chem. Phys.*, 13, 3547-3567,  
929 doi:10.5194/acp-13-3547-2013, 2013.

930 Zatzko, M.C., Geng, L., Alexander, B., Sofen, E.D., and Klein, K.: The impact of snow nitrate photolysis on  
931 boundary layer chemistry and the recycling and redistribution of reactive nitrogen across Antarctica  
932 and Greenland in a global chemical transport model, *Atmos. Chem. Phys.*, 16, 2819-2842,  
933 doi:10.5194/acp-16-2819-2016, 2016.

934 Zeller, E.J., Dreschhoff, G.A., and Laird, C.M.: Nitrate flux on the Ross Ice Shelf, Antarctica and its  
935 relation to solar cosmic rays, *Geophys. Res. Lett.*, 13, 1264-1267, 1986.

936

937

938 **Table 1.** Snowpit information on the traverse from coastal Zhongshan Station to Dome A, East  
 939 Antarctica.

Snowpit No.	Latitude, °	Longitude, °	Elevation, m	Distance to coast, km	Annual snow accumulation, kg m <sup>-2</sup> a <sup>-1</sup> )	Depth, cm	Sampling resolution, cm	Sampling year
SP1	-70.52	76.83	1613	132	193.2	150	5.0	2010/2011
SP2	-71.13	77.31	2037	200	172.0	150	3.0	2012/2013
SP3	-71.81	77.89	2295	283	99.4	200	5.0	2012/2013
SP4	-72.73	77.45	2489	387	98.3	200	5.0	2012/2013
SP5	-73.40	77.00	2545	452	90.7	200	5.0	2012/2013
SP6	-73.86	76.98	2627	514	24.6	300	2.5	2012/2013
SP7	-74.50	77.03	2696	585	29.2	100	2.0	2012/2013
SP8	-74.65	77.01	2734	602	80.2	180	2.0	2010/2011
SP9	-76.29	77.03	2843	787	54.8	200	2.0	2012/2013
SP10	-76.54	77.02	2815	810	100.7	240	3.0	2010/2011
SP11	-77.13	76.98	2928	879	81.2	200	2.5	2012/2013
SP12	-77.26	76.96	2962	893	83.4	265	5.0	2009/2010
SP13	-77.91	77.13	3154	968	33.3	200	2.0	2012/2013
SP14	-78.34	77.00	3368	1015	87.6	216	3.0	2010/2011
SP15	-78.35	77.00	3366	1017	70.0	162	2.0	2009/2010
SP16	-79.02	76.98	3738	1092	25.4	200	2.5	2012/2013
SP17	-79.65	77.21	3969	1162	46.2	130	2.0	2010/2011
SP18	-80.40	77.15	4093	1250	24.2	300	2.0	2010/2011
SP19	-80.41	77.11	4092	1254	23.7	300	1.0	2009/2010
SP20	-80.42	77.12	4093	1256	23.5	300	2.5	2012/2013
Core 1 <sup>2)</sup>	-70.83	77.08	1850	168	127.0	-	-	1996/1997
Core 2 <sup>3)</sup>	-76.53	77.03	2814	813	101.0	-	-	1998/1999

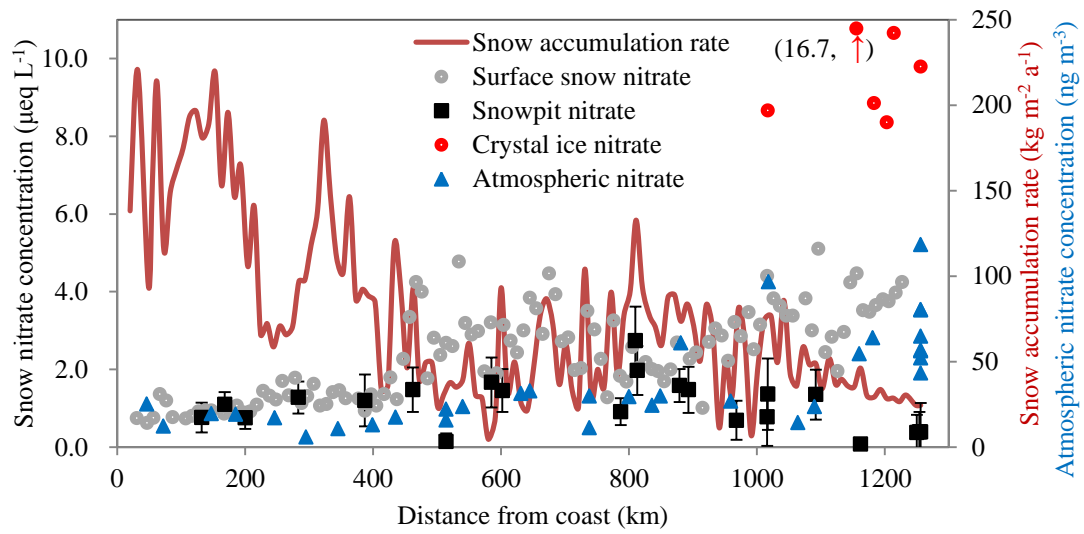
940 1) Annual snow accumulation rate is obtained from the field bamboo stick measurements (2009 - 2013),  
 941 updated from the report (Ding et al., 2011). Note that snow accumulation rate at the two ice core sites  
 942 are derived from ice core measurements.

943 2) Core 1, ice core data of previous report (Li et al., 1999; Xiao et al., 2004).

944 3) Core 2, ice core data of previous report (Li et al., 2009).

945

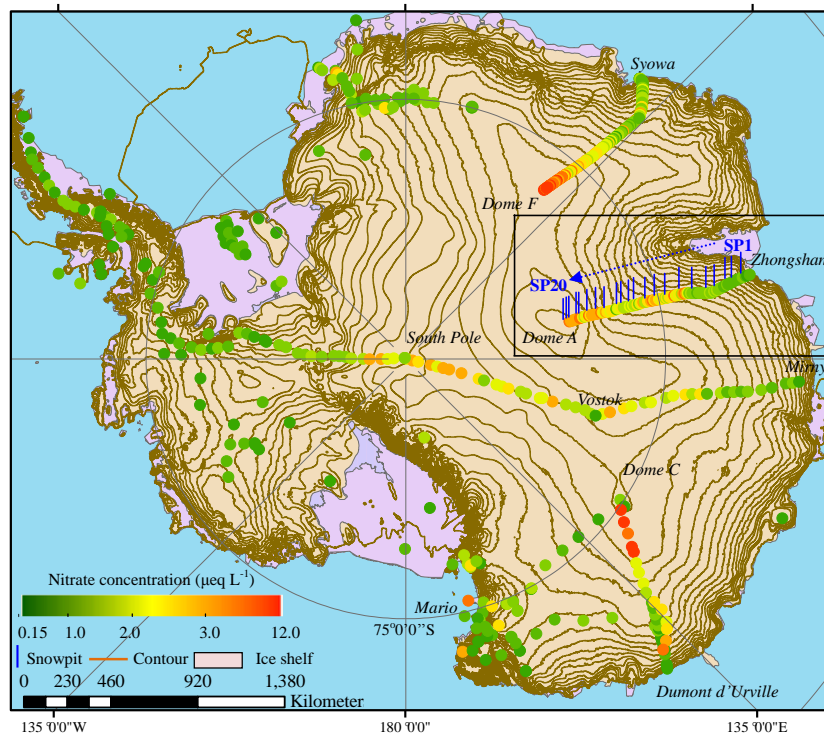




947

948 **Figure 1.** Concentrations of  $\text{NO}_3^-$  in snow (surface snow, crystal ice and snowpits; on the primary  
 949 y-axis) and atmosphere (on the secondary y-axis), with error bars representing one standard deviation  
 950 of  $\text{NO}_3^-$  ( $1\sigma$ ) for individual snowpits. Also shown is the annual snow accumulation rate on the traverse  
 951 (red solid line; based on Ding et al. (2011)). Note that  $\text{NO}_3^-$  concentration in one crystal ice sample (red  
 952 dot) is higher than the maximum value of the primary y-axis ( $\text{NO}_3^-$  concentration =  $16.7 \mu\text{eq L}^{-1}$  in the  
 953 parentheses).

954

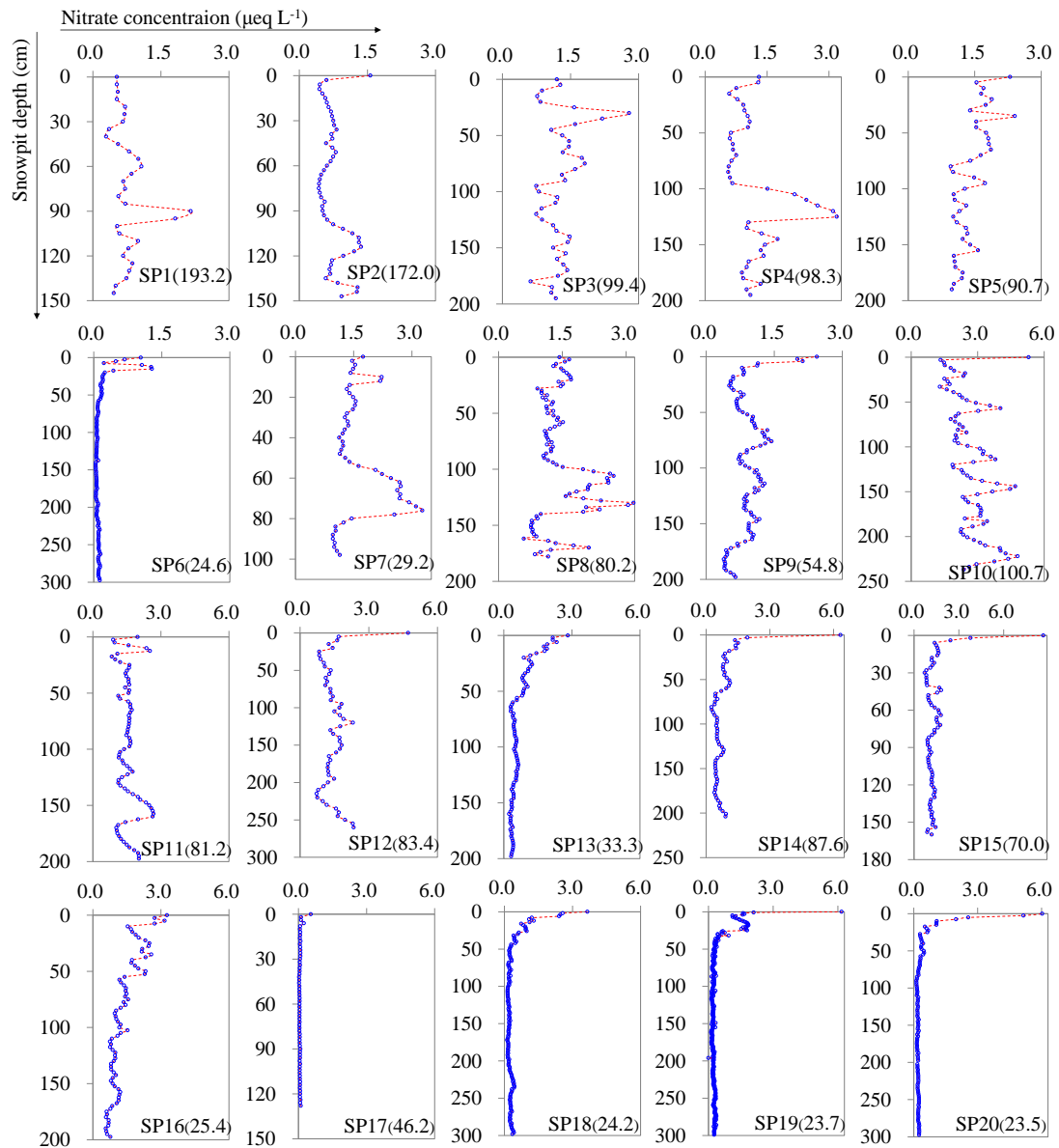


956

957

**Figure 2.** Concentrations of  $\text{NO}_3^-$  in surface snow across Antarctica. Note that the values of crystal ice  
 958 around Dome A were not included. The data of DDU to Dome C is from Frey et al. (2009). The other  
 959 surface snow  $\text{NO}_3^-$  concentrations are from compiled data (Bertler et al., 2005 and references therein).  
 960 Also illustrated are the locations of snowpits on the traverse route from Zhongshan to Dome A in this  
 961 study (SP1 to SP20, solid short blue line; Table 1).  
 962

962

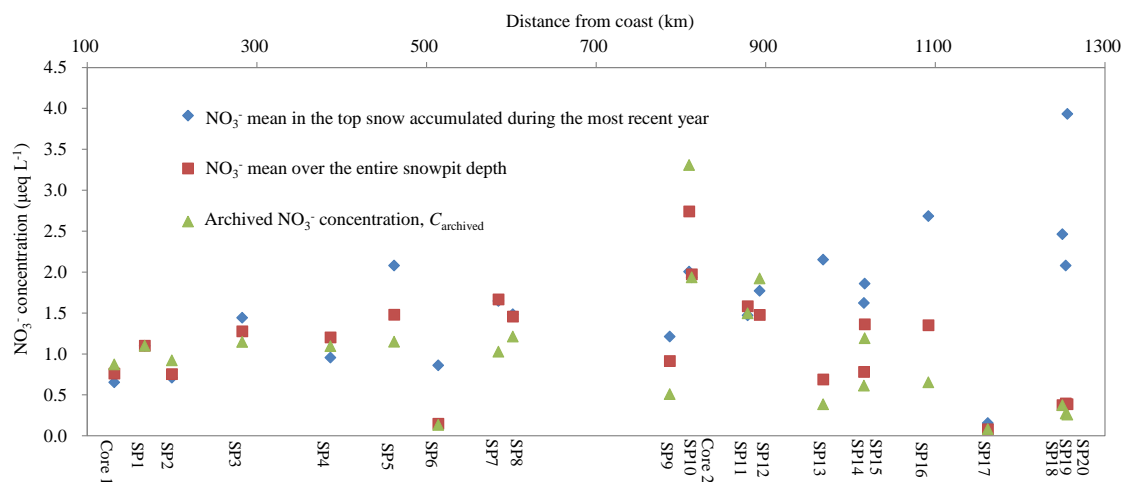


964

965 **Figure 3.** The full profiles of  $\text{NO}_3^-$  concentrations for snowpits collected on the traverse from the coast  
 966 to Dome A, East Antarctica (SP1 is closest the coast; SP20 the furthest inland; see Figure 2). The  
 967 details on sampling of the snowpits refer to Table 1. The numbers in parentheses in each panel denote  
 968 the annual snow accumulation rates ( $\text{kg m}^{-2} \text{a}^{-1}$ ). Note that the scales of x-axes for the snowpits SP1 –  
 969 SP9 and SP10 – SP20 are different.

970

971



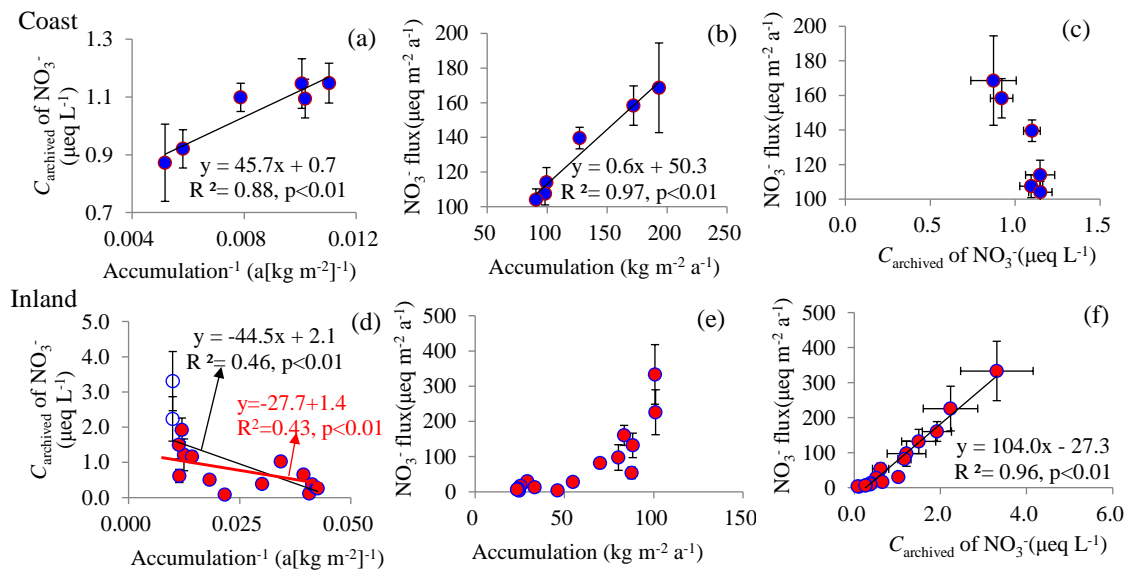
972

973 **Figure 4.** Mean concentrations of  $\text{NO}_3^-$  for the entire snowpit depth (in square), the uppermost layer

974 covering one-year snow accumulation (in diamond) and the bottom layer covering a full annual cycle

975 of deposition (archived  $\text{NO}_3^-$  concentration,  $C_{\text{archived}}$ , in triangle).

976



978

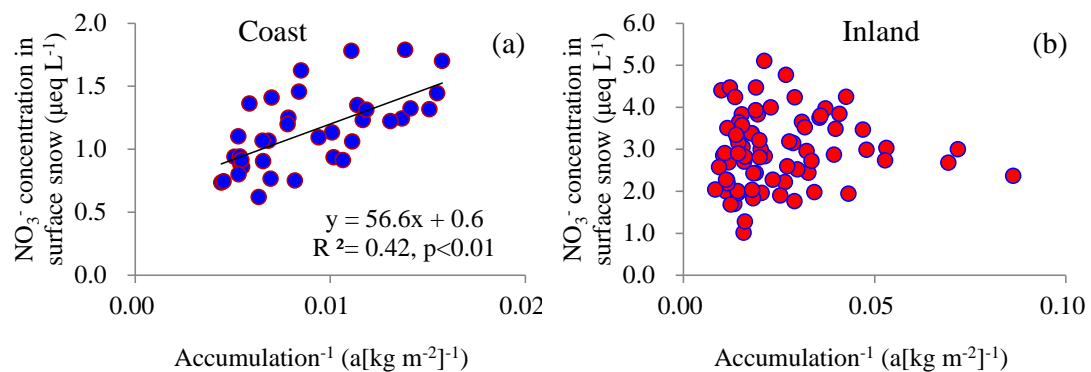
979

980 **Figure 5.** The relationships amongst snow accumulation rate, the archived concentration ( $C_{\text{archived}}$ ), and  
 981 flux of  $\text{NO}_3^-$  in coastal (top row, (a), (b) and (c)) and inland (bottom row, (d), (e) and (f)) Antarctica. In  
 982 panel (d), the linear fit in black line ( $y = -44.5x + 2.1$ ) includes the full data set, while the linear  
 983 equation in red ( $y = -27.7x + 1.5$ ) was obtained by excluding two cases (open circles) with snow  
 984 accumulation rate larger than  $100 \text{ kg m}^{-2} \text{ a}^{-1}$  (see the main text). The flux values are the product of  
 985  $C_{\text{archived}}$  of  $\text{NO}_3^-$  and snow accumulation rate, namely the archived flux. Least squares regressions are  
 986 noted with solid lines and are significant at  $p < 0.01$ . Error bars represent one standard deviation ( $1\sigma$ ).

986

987

988

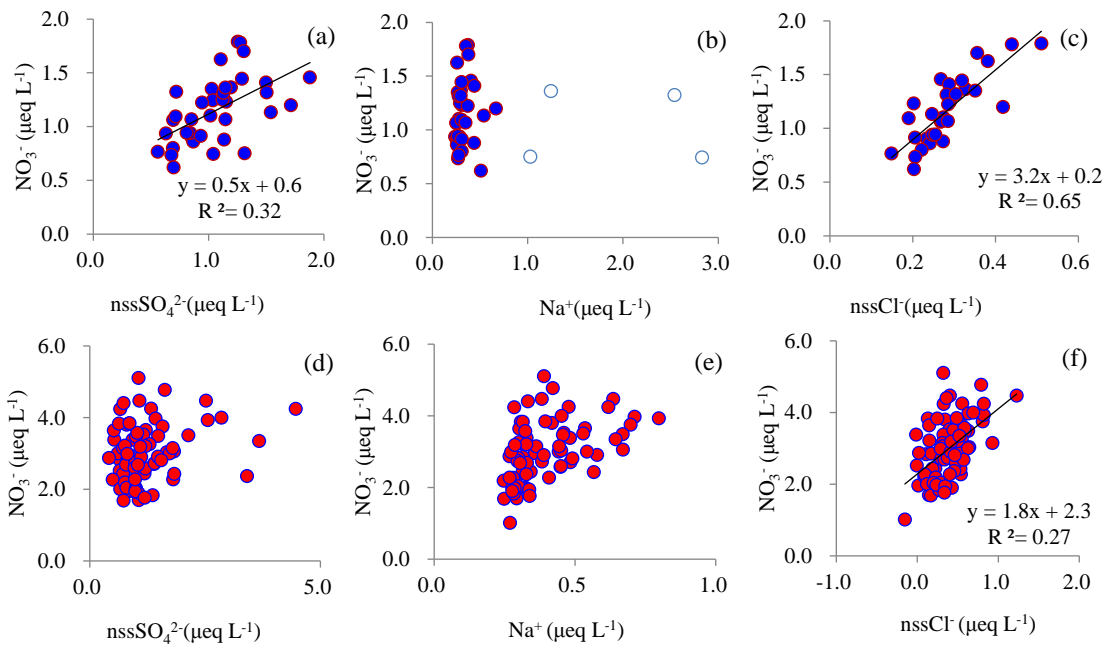


989

990 **Figure 6.** The relationships between  $\text{NO}_3^-$  concentration and inverse snow accumulation rate in surface  
991 snow in coastal (panel (a)) and inland (panel (b)) Antarctica. Least squares regressions are noted with  
992 solid line and are significant at  $p < 0.01$ .

993

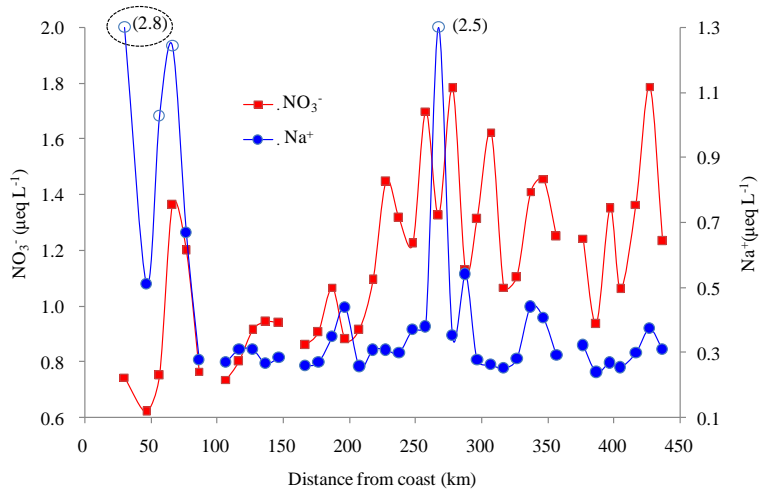
994



995

996 **Figure 7.** Relationships between  $\text{NO}_3^-$  and co-existing major ions in surface snow in coastal (top row,  
997 (a), (b) and (c)) and inland (bottom row, (d), (e) and (f)) Antarctica. Least squares regressions are noted  
998 with solid line and are significant at  $p < 0.01$ . The 4 samples with high  $\text{Na}^+$  concentrations are denoted  
999 by blue open circles (b), the same as those in Figure 8 (the blue open circles). Note that the 4 samples  
1000 were excluded in the plot of  $\text{NO}_3^-$  vs.  $\text{nssCl}^-$  (c).  
1001

1002



1003

1004

1005

1006

1007

1008

1009

**Figure 8.** Concentrations of  $\text{NO}_3^-$  and  $\text{Na}^+$  in surface snow samples on the coast. Four samples with high  $\text{Na}^+$  concentrations are denoted by open circles, corresponding to those in Fig. 7b. Note that  $\text{Na}^+$  concentrations in two samples, 2.5 and 2.8  $\mu\text{eq L}^{-1}$  in parentheses, are above the maximum value of the secondary y-axis ( $\text{Na}^+$  concentration). The sample in the dashed ellipse, with  $\text{Na}^+$  concentration of 2.8  $\mu\text{eq L}^{-1}$ , is the fresh snowfall.